Pergamon

Geochimica et Cosmochimica Acta, Vol. 67, No. 7, pp. 1259–1276, 2003

0016-7037/03 $30.00 + .00

doi:10.1016/S0016-7037(02)01292-9

Hydrogen isotope exchange kinetics between H_2O and H_4SiO_4 from ab initio calculations

M. A. Felipe,[1,*] J. D. Kubicki,[2] and D. M. Rye[1]

[1]Department of Geology and Geophysics, Yale University, New Haven, CT 06511 USA
[2]Department of Geosciences, The Pennsylvania State University, University Park, PA 16802 USA

(*Received December* 27, 2001; *accepted in revised form October* 22, 2002)

Abstract—Hydrogen isotope exchange between water and orthosilicic acid (H_4SiO_4) was modeled using B3LYP calculations and classical transition-state theory. Configurations of 1, 2, 3 and 7 water molecules and H_4SiO_4 were used to investigate energetically viable reaction pathways. An upper-bound of 71 kJ/mol was assumed for the zero-point energy corrected barrier (ZPECB) because this is the experimentally determined activation energy for Si-O bond breaking (Rimstidt and Barnes, 1980) and ZPECB is expected to be close to this value. Long range solvation forces were accounted for using the integral equation formalism polarized continuum model (IEFPCM; Cancès et al., 1997). Primary and secondary isotope effects were computed by exchanging hydrogen atoms with deuterium. Results show that reaction mechanisms involving 3 and 7 water molecules have ZPECB of 34 to 38 kJ/mol, whereas those involving 1 and 2 water molecules have ZPECB in excess of the set upper-bound. The lower range of ZPECB with 3 or 7 water molecules is reasonable to explain rapid hydrogen isotope exchange with silicates. Rate constant calculations accounting for tunneling, anharmonicity and scaling factors indicate that the reaction is fast and equilibrium can be assumed under most geologic conditions.

1. INTRODUCTION

Isotope geochemists frequently make either the explicit or implicit assumption that the species in solution undergo isotope exchange with water on time scales much shorter than the time scales of fluid transport or fluid rock exchange. This assumption allows the use of the isotopic composition of precipitates from water and species bound within the lattice structure of silicates as proxies for the isotopic fluid phase provided that the isotopic fractionation between the phase of interest and the fluid phase is known (e.g., Lasaga and Rye, 1993; Jenkin et al., 1994; Brandriss, 1998; Cole, 2000; Gotze, 2001; Jia et al., 2001). We have known for a long time that this assumption breaks down for a number of geologically relevant systems, such as isotopes of oxygen in phosphates and sulfates (Lloyd, 1968; Longinelli and Nuti, 1968; Blake et al., 1997; Lecuyer et al., 1999). We can therefore envision two end member cases that can exist for isotopes of dissolved species in general. At one end of the spectrum, the isotopes can reflect the solution water, and at the other end of the spectrum they can reflect their source. In between, isotopes can take part in a number of competing reactions and can contribute to a dynamic process controlled by the rates of the competing reactions.

Making direct measurements of isotopic species in solution is difficult at best. As a consequence we have embarked on a series of ab initio calculations to determine both the magnitude of isotopic fractionations and the rates of isotopic reactions between fluids and species in solution. Ab initio numerical simulations of exchange reactions provide an alternative, direct and independent means to elucidate the mechanisms of reactions. Results derived from such calculations have gained wider acceptance recently in different fields of chemistry as well as in industry due to their proven predictive power (See Cygan and Kubicki, 2001 for a review). In the first of these papers, we consider the hydrogen isotopic exchange between silicic acid and water. We expect the rates to be fast and the acid to reflect the water directly. Nevertheless, without the carrying out this "experiment" there can be no certainty that this expectation is true. This undertaking could have profound implications on our understanding of any reaction that involves the hydrogen on the silicic acid directly. It should be emphasized though that hydrogen atoms bound within the lattice structure of silicates possibly have various origins, such as dissolved species, hydrogen bearing minerals and water. Thus, finding the rate of hydrogen isotope exchange between orthosilicic acid and water mainly tells us about orthosilicic acid composition with time and not incorporated hydrogen isotopes directly.

The isotopes of hydrogen, ^1H (protium) and ^2H (or D, deuterium), are used extensively in studies where water either interacts with rock material or evolves from a source body (Shieh and Taylor, 1969; Taylor, 1974; Taylor, 1979; Taylor and Forester, 1979; Campbell et al., 1984; Ohmoto, 1986). These isotopes, along with isotopes of other elements such as oxygen and carbon, are used to characterize different types of water, water-to-rock mass ratios, and fluid travel times (see Valley, 1986). As a result, there is a wealth of information on the fractionation of hydrogen isotopes between H-bearing minerals and water (Taylor, 1979; Dobson et al., 1989) and new methods are actively being developed to extract these information (Vennemann and ONeil, 1996; Chacko et al., 1999; Xu and Zheng, 1999). In contrast, geochemical studies regarding the rates and mechanisms of isotopic (or even simply atomic) exchange are rare (Gregory et al., 1989; Lecluse and Robert, 1994; Guo and Qian, 1997; Krishnamurthy and Machavaram, 1998; Xu and Stebbins, 1998; Casey et al., 2000; Cole, 2000; Faiia and Feng, 2000). In fact, we have not been able to find a single study on the kinetics of H-isotope exchange between water and aqueous silica. This may be due to the fact that H-isotope exchange rates are likely to be fast compared to most

* Author to whom correspondence should be addressed (mihali.felipe@yale.edu).

geochemical processes and the fact that silica is sparingly soluble in water under ambient conditions.

Hydrogen exchange-reaction mechanisms between water molecules and various compounds have been the subject of numerous recent ab initio molecular modeling studies. The transferability of protons in water itself has been the focus of considerable effort (e.g., Luth and Scheiner, 1992; Lobaugh and Voth, 1996; Geissler et al., 2001). These are closely related to studies dealing with water clusters (Khan, 1999; Hodges and Stone, 1999) and investigations of proton transfer mechanisms from inorganic acids such as acid halides to water (Ando and Hynes, 1997). In addition, a series of modeling studies have been conducted (Casey et al., 1990; Lasaga, 1992; Xiao and Lasaga, 1994) recently which focus on hydrolysis of T-*O*-T linkages and dissolution of silica or aluminosilicates. Proton transfer between H_2O or H_3O^+ is a critical step in each of these studies. The objective of this study is to investigate the mechanism of hydrogen exchange (i.e., proton transfer) between orthosilicic acid and water and quantify the order of magnitude of the rates. From the conclusions on the mechanism and kinetics of isotope exchange in H_4SiO_4 and H_2O, inferences can also be drawn on the exchange of hydrogen isotopes between silica surfaces and water because silanols (Si-OH) are involved in both cases.

2. THEORY

In this study, we make use of the concepts of classical transition-state theory (TST) and potential energy surfaces calculated with molecular orbital (MO) theory. The method that makes use of the combination of these two theories will be referred to as MO-TST. We shall briefly discuss the salient points of these two theories, especially as they relate to the reaction kinetics of isotope exchange.

Consider the hypothetical elementary exchange reaction in the condensed phase

$$H_4SiO_4 - DOH \Leftrightarrow [\text{Transition State}] \Leftrightarrow H_3DSiO_4 - HOH \tag{1}$$

wherein the isotope exchange reaction is treated as a unimolecular structural isomerization event (i.e., no collision or diffusion of the reactants necessary). This assumption is justifiable for solutes exchanging isotopes with H_2O in aqueous solution, because, in this case, the H_4SiO_4 solute is at all times surrounded by H_2O solvent molecules (e.g., Shmulovich et al., 2001). Furthermore, experiments and molecular dynamics simulations show that liquid water consists of hydrogen bonded clusters of H_2O (Stanley and Teixeira, 1980; Gregory et al., 1997; Mishima and Stanley, 1998) and therefore clusters of several water molecules are abundantly available. If we approximate the system by a harmonic oscillator treatment, the TST rate constant for this reaction can be given by (Eyring, 1957 see Lasaga, 1981; 1998)

$$k_f = \frac{k_B T}{h}\frac{Q^{\ddagger}}{Q_{H_4SiO4-DOH}}\exp\left(\frac{-\Delta\varepsilon_o}{k_B T}\right) = \frac{k_B T}{h}\frac{[q_{vib}q_{elec}]^{\ddagger}}{[q_{vib}q_{elec}]_{H_4SiO4-DOH}}\exp\left(\frac{-\Delta\varepsilon_o}{k_B T}\right) \tag{2}$$

for the forward direction, where k_B is Boltzmann's constant, T is the temperature, h is Planck's constant, Q_i are generalized partition functions (McQuarrie, 1973), the superscript‡ refers to the transition state, $\Delta\varepsilon_o$ is the difference of zero-point energies between the reactant and the transition state, q_{vib} and q_{elec} are partition functions for vibrations and electronic states, respectively. The rate constant for the reverse reaction can analogously be rendered. In general, the TST rate constant is meaningful if the frequency of adsorption of water to silicic acid and the diffusion and transport of water to orthosilicic acid are not rate limiting. Studies have shown that there are no potential energy barriers in the formation of H-bonds in water (Odutola and Dyke, 1980; Rybak et al., 1991; Rodriguez et al., 1999) and adsorption of H_2O onto H_4SiO_4 (Lasaga and Gibbs, 1990; Xiao and Lasaga, 1994; Pelmenschikov et al., 1997). Hence, if the isotope exchange occurs at a fast enough rate as we expect it to be, then the rate limiting process is the diffusion and transport of water.

In our unimolecular treatment, the relative translations and rotations between the water and orthosilicic acid units are omitted and instead are accounted for as vibrations (i.e., all internal degrees are partitioned to vibrations). By invoking the known values of the classical partition functions (e.g., McQuarrie, 1973), the rate constant for Eqn. 2 can be simplified to

$$k_f = \frac{k_B T}{h}\prod_i^{3N-6}(1 - \exp(-h\nu_i/k_B T)) \cdot \prod_i^{3N-7}\left(1 - \exp(-h\nu_i^{\ddagger}/k_B T)\right)^{-1}\exp\left(\frac{-\Delta E_o}{k_B T}\right) \tag{3}$$

which we shall refer to as the *absolute rate constant* (ARC) equation. We remind the reader that this is not the rate of the reaction but the rate constant (i.e., where $Rate = k_f[A]$ for a first order reaction). Here, ν_i are vibrational frequencies and N is the number of nuclear centers. The ZPECB, which is denoted by ΔE_o, are computed using the zero-point energies of the transition state and the reactant, and their calculated potential energies

$$\Delta E_o = \varepsilon^{\ddagger} + \varepsilon_o{}^{\ddagger} - \varepsilon_{rct} - \varepsilon_{rcto} = \varepsilon^{\ddagger} - \varepsilon_{rct} - \Delta\varepsilon_o. \tag{4}$$

The potential energies of the transition-state and reactants, $\varepsilon^{\ddagger}$ and ε_{rct}, are taken from the potential energy surface (PES); whereas, the zero-point energy corrections, $\varepsilon_o{}^{\ddagger}$ and ε_{rcto}, are obtained by performing summations over the normal-modes (from frequency calculations; see Foresman and Frisch, 1996) on the transition-state and reactant configurations, that is,

$$\varepsilon_o{}^{\ddagger} = \sum_i \frac{1}{2}h\nu_i^{\ddagger} \quad \varepsilon_{rcto} = \sum_i \frac{1}{2}h\nu_{rcti} \tag{5}$$

where $\nu_i^{\ddagger}$ and ν_{rcti} are vibrational frequencies of the transition state and reactants respectively.

We may therefore evaluate the forward and reverse rate constants, k_f and k_r, using Eqn. 3 by considering the forward and reverse reaction if we know the configurations and energies of the reactants, products and the transition states. These configurations can be computed using ab initio calculations. In this

study, a density functional theory (DFT; Hohenberg and Kohn, 1964; Kohn and Sham, 1965) method with a hybrid functional is utilized to determine the potential energy surfaces (Foresman and Frisch, 1996). DFT calculations are useful for taking electron correlation into account without dramatically increasing the computational time.

The rate constants computed using the unimolecular harmonic oscillator model assumption, and hence ARC (Eqn. 3), may be used as a baseline in evaluating the accuracy of the model. We use this approach by way of necessity: while there may be spectra for some of the vibrational modes of our reactants and products, it should be pointed out that transition states are merely theoretical constructs by definition and therefore we do not expect spectra for these to be available. We shall however address errors in the vibrational modes through scaling factors. We evaluate the accuracy of the reference unimolecular harmonic oscillator model rate constants by comparing them with rate constants that account for quantum tunneling effects, scaling factors, and anharmonicity. We explore enhancements using an implicit solvation model, which we describe in the Methodology section below. Furthermore, we attempt to evaluate the DFT method by comparing it with results from the second-order Møller-Plesset (MP2) method.

For light atoms such as hydrogen and its isotopes, quantum tunneling effects may be appreciable. These corrections to the rate constant are in the form of a correction factor κ such that

$$k_{f,corr} = \kappa k_f \tag{6}$$

where $k_{f,corr}$ is the corrected rate constant. There are various suggested expressions for κ, the simplest and most common being the first order Wigner treatment (Wigner, 1937)

$$\kappa = 1 + \frac{1}{24}\left|\frac{h\nu^{\ddagger}}{k_B T}\right|^2 \tag{7}$$

where $\nu^{\ddagger}$ is the imaginary vibrational frequency at the saddle point. This correction assumes a parabolic potential surface at the saddle point, and is only valid if certain conditions are satisfied. First, the contributions to tunneling must only come from the saddle point region of the PES where transverse modes do not vary appreciably. Second, the PES curvature should also be that of a concave down parabola (Truhlar et al., 1985). Third, the calculations should be at reasonably high temperatures, (e.g., $>$ 298K) (Truong, 1997). Calculations on some gas phase systems have shown that Wigner tunneling corrections underestimate the rate constants at low temperatures (Truong, 1997).

A more sophisticated expression of κ assumes an Eckart potential surface (Eckart, 1930). The tunneling correction is given by

$$\kappa = \left(\frac{1}{k_B T}\right)\int_{-\Delta E_{o,f}}^{\infty} P(E)\exp(-E/k_B T)dE \tag{8}$$

where the tunneling probability *P(E)* may be given by (Miller, 1979)

$$P(E) = \frac{\sinh(a)\sinh(b)}{\sinh^2\left(\frac{a+b}{2}\right) + \cosh^2(c)} \tag{8a}$$

and the parameters a, b, and c are given by

$$a = \frac{4\pi}{h\nu^{\ddagger}}\frac{(E+\Delta E_{o,f})^{1/2}}{(1/\Delta E_{o,f}^{1/2}) + (1/\Delta E_{o,r}^{1/2})} \tag{8b}$$

$$b = \frac{4\pi}{h\nu^{\ddagger}}\frac{(E+\Delta E_{o,r})^{1/2}}{(1/\Delta E_{o,f}^{1/2}) + (1/\Delta E_{o,r}^{1/2})} \tag{8c}$$

and

$$c = 2\pi\left(\frac{\Delta E_{o,f}\Delta E_{o,r}}{(h\nu^{\ddagger})^2} + \frac{1}{16}\right) \tag{8d}$$

The subscripts "*f*" and "*r*" are used to indicate the forward and reverse reaction ZPECB and *E* is a dummy variable for the energy in the integral. The integral is readily solved by numerical integration. Calculations on some gas phase systems show that Eckart tunneling corrections overestimate the rate constant at low temperatures (Truong, 1997). We use the Wigner and Eckart tunneling corrections as indicators of the order of magnitude that tunneling might contribute to the rate constant.

It has been demonstrated that the vibrational frequencies and zero-point energies systematically vary with the MO method and that scaling factors need to be incorporated for frequencies and zero-point energies to be comparable with empirical data (Pople et al., 1993; Scott and Radom, 1996). These scaling factors express themselves as coefficients to the vibrational frequencies and concomitantly the zero-point energy corrections. We treat these scaling factors as generalized errors of the harmonic oscillator approximation. This is a convenient way of accounting for the vibrational errors without individually treating the vibrational modes.

A critical assumption in the evaluation of rate constants using Eqn. 2 is that the system can be modeled by a set of independent harmonic oscillators corresponding to the normal modes; this simplification is for practical purposes, and whether this is a valid assumption is debatable. (The true test of its validity is its agreement with empirical data.) In theory, several enhancements could be performed but these require parameters and constants (anharmonicity constants, centrifugal distortion constants, rotation-vibration coupling constants, etc.; see McQuarrie, 1973) that are unavailable for our system of interest. We explore potential errors introduced by the harmonic oscillator treatment by comparing it with results using the anharmonic oscillator partition function. Recall that in Eqn. 2

$$q_{vib} = \prod_i^{3N-S} q_{vib,i} = \prod_i^{3N-S}(1-\exp(-h\nu_i/k_B T))^{-1} \tag{9}$$

where S = {6 for a minimum; 7 for a transition state}. The anharmonic oscillator partition function q_{anh} is similarly given by (Houston, 2001)

$$q_{anh} = \prod_i^{3N-S} q_{vib,i}\left(1 + \frac{h\chi_i\upsilon_i}{kT}\left(\frac{1}{4} + 2q_{vib,i}^2\right)\right) \tag{10}$$

where $\chi_i\nu_i$ are the anharmonicity constants. Substituting q_{anh}

for q_{vib} in Eqn. 2 will yield rate constants within the unimolecular anharmonic oscillator assumption.

In many cases, it is worthwhile to relate computed kinetic parameters to measured thermodynamic quantities. For example, the equilibrium constant for an elementary reaction can be evaluated using the principle of microscopic reversibility (Onsager, 1931)

$$K_{eq} = \frac{k_f}{k_r} \tag{11}$$

Note that K_{eq} is an entirely thermodynamic entity and the transition state contributions in the form of partition functions are cancelled out in Eqn. 11. However, we can deduce an important aspect of the reaction kinetics by evaluating K_{eq}. If K_{eq} does agree with experimental data, then this strongly suggests that the *elementary* reaction determined is indeed a *full* reaction. However, if it does not, then either the model system is incorrect, the data used in computing the partition functions is inaccurate, or the mechanism found is merely part of a multi-step equilibrium reaction.

Fractionation factors for isotopic exchange reactions (O'Neil 1986) can be computed as well, using the following relationship between α and K_{eq}

$$\alpha = K_{eq}^{1/x} = \frac{\left(\frac{D}{H}\right)_{H_2O}}{\left(\frac{D}{H}\right)_{H_4SiO_4}} = \frac{[H]_{H_4SiO_4}}{[H]_{H_2O}} \frac{[D]_{H_2O}}{[D]_{H_4SiO_4}}$$

$$= \left(\frac{k_r}{k_f}\right)_H \left(\frac{k_f}{k_r}\right)_D = \left(\frac{k_f}{k_r}\right)_D \tag{12}$$

where the square brackets represent concentrations of species in moles/L, the number of isotopes exchanged x = 1, and the indices D and H refer to the deuterated and undeuterated reaction. The ratio $(k_r/k_f)_H$ is unity because this is an equilibrium constant for a reaction with no net isotopic exchange. Note that the k_f and k_r are functions of T, and thus we are able to evaluate $\alpha(T)$. Therefore, we may be able to test our calculations against the $1000\ln(\alpha)$ vs. $1/T$ and $1/T^2$ plots prevalent in isotope geochemistry (O'Neil, 1986).

3. MATERIAL AND METHODS

The ab initio calculations were primarily carried out using gaussian 94 (Frisch et al., 1995) in a DEC Alpha 600au, and in two DEC Alpha XP1000's all running Compaq Tru64 UNIX. We have also utilized gaussian 98 (Frisch et al., 1998) in an Intel Pentium II running Linux 2.1, an Intel Pentium IV running Linux 2.4, and a 48 cpu HP SuperDome 9000/800 running HPUX 11.11. A MO-DFT method, in particular Becke's three-parameter method (Becke, 1993) with Lee-Yang-Parr functionals (Lee et al., 1988) or B3LYP, was mainly used to account for electron exchange and correlation. The reason for using DFT over other methods such as pure Hartree-Fock theory (HF) is that DFT considers electron-correlation and is expected to yield more accurate energetics than HF, which neglects electron correlation. Furthermore, DFT scales more efficiently with the size of the system than does HF theory or Møller-Plesset (MP) methods such as MP2 to MP5 (Møller and Plesset, 1934; Frisch et al., 1998 and refs. within). The B3LYP method is an accepted method for the silica-water system for determining reaction mechanisms (Hoshino and Nishioka, 1999; Walsh et al., 2000; Pelmenschikov et al., 2001) and thermochemistry (Civalleri et al., 1998; Sefcik and Goddard, 2001). Ground state structures using this method have been shown to be reliable for small molecules from hydrogen to argon (Janoschek, 2001).

Extended ((d) or (d,p)) and diffuse (+) basis sets, 3–21G(d), 6–31G(d) and 6–31+G(d,p) (Hehre et al., 1972; Binkley et al., 1980; Gordon et al., 1982), were used to build the singlet state electron wavefunctions of the molecular configurations. Optimizations were performed in each of these levels, sequentially in increasing wavefunction basis set size, using the optimized result from the lower levels as input for the next higher level.

Systems of $H_4SiO_4 + nH_2O$ (n = 1, 2, 3, 7) were chosen to represent dissolved silica in water. Inclusion of an increasing number of water molecules was chosen as a method of testing system size effects and the role of H-bonding in these model reactions. Note that these H_2O molecules are not all strictly stoichiometric waters of hydration (i.e., n is not necessarily the coordination number) as described by Shmulovich et al. (2001) but are chance configurations of water molecules around the H_4SiO_4. Once a reaction mechanism with reasonably low ZPECB was found, the next exploration made was explicit hydration. Therefore, the choices for n are the result of the progress of the study rather than predetermined at the onset. Explicit hydration was accomplished using the addition of a known conformation of H_2O clusters (Gregory et al., 1997; Rodriguez et al., 1999).

Local energy minima within the vicinity of the purported starting and ending configurations were then sought using standard methods as outlined by Peng et al. (1994). These potential energy minima correspond to prospective reactants, products and intermediates of the reactions of interest. Having computed the local minima, the first-order saddle points that link them were then sought. These first-order saddle points correspond to the transition states of reaction mechanisms and are similar to energy minima except a slight change along one particular direction lowers the energy; this one direction is the reaction coordinate. A full reaction mechanism is defined by a pair of local minima (reactants, and products or intermediates), and a first-order saddle point (transition state) linking the two. The process of finding these stationary points is often referred to as "full optimization," and leads to a "fully optimized configuration."

In these calculations, problems such as basis-set superposition errors (BSSE; Sauer, 1989) and size consistency (Hehre et al., 1986) are minimal because all energy differences are computed using reactant, transition-state and product configurations that have the same stoichiometry and very similar geometries. The reactions are treated unimolecularly and the constituent molecules are never treated as isolated entities. Therefore, these calculations make use of the same basis set and the same number of basis functions with minimal basis set superposition differences. Furthermore, corrections suggested in the literature such as the counterpoise method (Boys and Benardi, 1970) are only approximate and may in this case overestimate and eventually lead to a larger error than not making corrections at all (H. B. Schlegel, private communication).

Note that in our unimolecular treatment, translations and rotations of reactants relative to each other are treated as vibrations. In other words, the $3N$-6 internal degrees of freedom for energy minima (because all configurations considered are nonlinear) and $3N$-7 internal degrees of freedom for transition states are all accounted for as vibrations. Since we are modeling a condensed phase reaction, there may be hindered rotations and translations for the entire system. However, these are approximately cancelled out in the calculation of the rate constants because the angular momenta (and hence, the rotational partition function) are not expected to change significantly, and the total masses (and hence, translational partition function) do not change from reactants to transition state.

The method used to search for the transition states is a combination of the "reaction-coordinate approach" (or "constrained optimization") (McIver and Kormonicki, 1972; Foresman and Frisch, 1996) and either the synchronous-transit quasi-Newton method (STQN) (Peng and Schlegel, 1994), or a Berny optimization (Frisch et al., 1998). The "reaction-coordinate approach" is accomplished by constraining one degree of freedom stepwise, while optimizing the remaining degrees of freedom. Whenever successful, the reaction-coordinate approach yields a locus of "partially optimized" points in potential energy space between the pairs of local minima. An automated procedure, used in conjunction with gaussian 94 and gaussian 98, was designed to perform this task. Searches were aborted when the energy difference between

the constrained configuration and the nearest local minimum, that is the uncorrected energy barrier, exceeded 71 kJ/mole, which is within the empirically determined Si-O bond breaking activation energy range (Rimstidt and Barnes, 1980; Dove and Crerar, 1990; Dove, 1994; Icenhower and Dove, 2000). (It is assumed that the energy barrier would be close in value to the experimentally determined activation energies because the latter are usually determined by performing linear regressions of -ln(k) versus 1/T plots and getting the slope. Therefore, what is actually determined experimentally is an activation energy over a temperature range.) Above the set threshold, H isotope exchange rates would correlate with O isotope exchange rates because O exchange for this system would imply an abstraction of an entire OH group.

After determining the locus of points connecting the pair of minima, a "transition-state optimization" is performed using the highest energy point on the locus as the first guess for the STQN or Berny calculation leading to a "transition-state optimized" configuration. The resulting optimized configuration is then checked (1) whether it is a true first-order saddle point, and (2) whether it is indeed the first-order saddle point connecting the reactants and products. We shall refer to these as the "reaction coordinate criteria." The first criterion is met when the computation of the vibrational frequencies for the transition-state leads to an imaginary vibrational frequency corresponding to the negative curvature. The second criterion is met when, after following the normal mode vector corresponding to the negative curvature in its positive and negative directions using the transition-state as the starting point, configurations closer to the products and reactants, respectively, are approached. In other words, the reaction path, beginning with the transition state, is followed along the two directions of the maximum energy decrease to determine if the desired reaction is indeed being followed.

After calculating the three configurations representing reactant, product and transition-state, vibrational analyses were performed to correct for zero-point energies. These calculations assume that the energy within the system is in the form of vibrations along normal modes. This is a reasonable approximation for simulations of condensed state reactions (see Drenth and Kwart, 1980).

System solvation was treated in two ways—explicit and implicit hydration. Explicit hydration is accomplished by adding discrete numbers of water molecules to the system. The intention was to simulate the solvation surrounding the -OH group. An advantage of explicit hydration is that it elucidates the nature of the H-bonding of water molecules near the orthosilicic acid OH. (Note that we did not model the solvation sphere around the entire H_4SiO_4 molecule, which would be more realistic but prohibitively time consuming.)

The second level of solvation is implicit using a polarized continuum solvation model. The numerical method utilized in this study, the integral equation formalism polarized continuum model (IEFPCM; Cancès et al., 1997), is a variation of the self-consistent reaction field (SCRF) methods that surround a solute with a polarizable continuum with a selected dielectric constant (see Keith and Frisch, 1994). In the IEFPCM approach, the overall neutral surface between the solute and the solvent is divided into a number of tesserae with an electric charge. Polarization of this continuum then occurs as the electron density from the solute molecule interacts with the surface charge distribution to lower the energy of the system as a whole. Generally, this is an iterative process that determines a solute electron density, then a surface charge distribution, then the solute electron density is re-calculated according to the new surface charge distribution. These iterations are continued until a self-consistent solution is found (hence, the terminology, self-consistent reaction field). The end result is to allow charge stabilization of the solute compared to a vacuum due to the ion-dipole and dipole-dipole interactions of the solute with the continuum similar to those in a solvent. IEFPCM accounts for long-range interactions and has been shown to be numerically stable (Cancès et al., 1997). The IEFPCM model neglects the energetics of forming the surface and the SCRF models in general do not account for specific H-bonds and short range dispersive interactions, so inclusion of explicit H_2O molecule interactions with the solute is desirable.

With the IEFPCM model, the ΔE_o is replaced by $\Delta E_{o,solv}(T)$ in Eqn. 3 where

$$\Delta E_{o,solv}(T) = \varepsilon^{\ddagger}_{solv}(T) - \varepsilon_{rct,solv}(T) - \Delta\varepsilon_o \qquad (13)$$

and the solvation corrected energies, $\varepsilon^{\ddagger}_{solv}(T)$ and $\varepsilon_{rct,solv}(T)$ are transition state and reactant energies taken from the solvation corrected potential energy surface. It should be emphasized that the ZPECB is ΔE_o and not $\Delta E_{o,solv}(T)$. Also, the experimentally determined activation energies are temperature dependent by definition and is closer in nature to $\Delta E_{o,solv}(T)$.

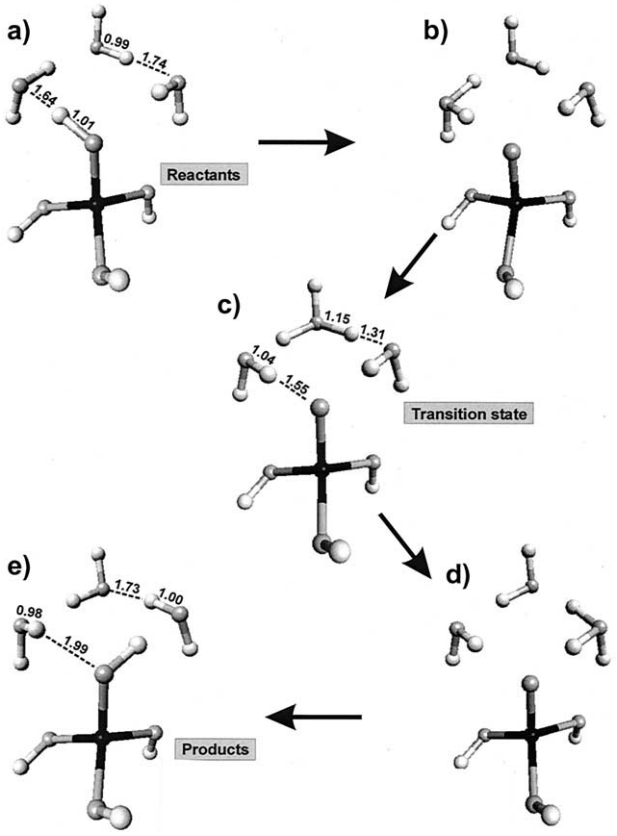

Fig. 1. Hydrogen isotope exchange reaction mechanism of the H_4SiO_4 + $3H_2O$ system at the B3LYP/6–31+G(d,p) level. The reaction involves one step. Si—black, O—grey, H—white.

4. RESULTS AND DISCUSSION

4.1. Mechanism and Implications for Kinetic Data

Given our methodology, particular reaction coordinates must be preselected that represent reasonable initial guesses for the reaction mechanism. To test that we were not picking an incorrect reaction coordinate, various constrained optimization paths were examined.

Parameters chosen to represent the "reaction coordinate" include the following: bond lengthening of O-H in H_4SiO_4; shortening of the H_2O to orthosilicic acid H—O distance; and shortening of water to water H—O distance, thereby forcing the former water molecule to become an acceptor of H^+ from H_4SiO_4. The lattermost constrained optimization path produced the desired H isotope exchange within the preset 71 kJ/mol upper bound. The first two pathways were abandoned after surpassing the upper bound. Successfully computed and complete specific reaction mechanisms for the n = 3 and n = 7 systems are illustrated in Figures 1 and 2. The end-members shown in Figures 1a, 1e, 2a and 2c are energy minima corresponding to reactants and products; the configurations shown in

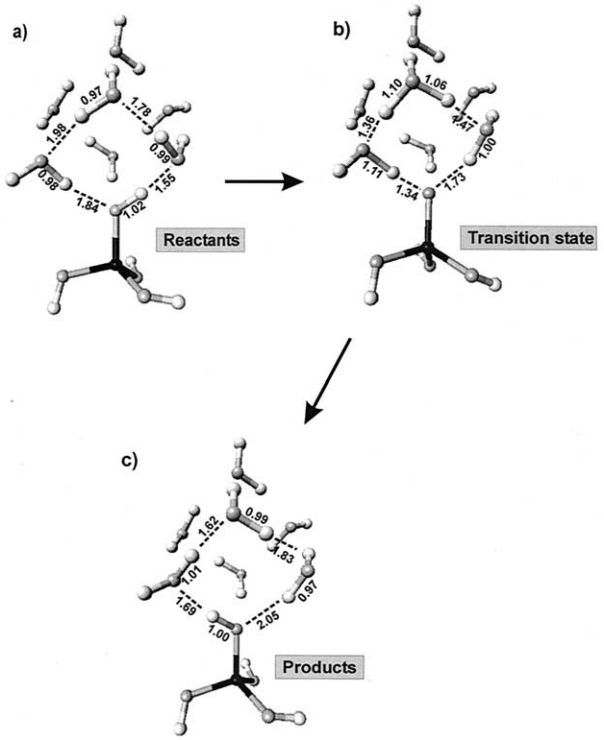

Fig. 2. Hydrogen isotope exchange reaction mechanism of the H_4SiO_4 + $7H_2O$ system at the B3LYP/6–31+G(d,p) level. The reaction involves one step. Si—black, O—grey, H—white.

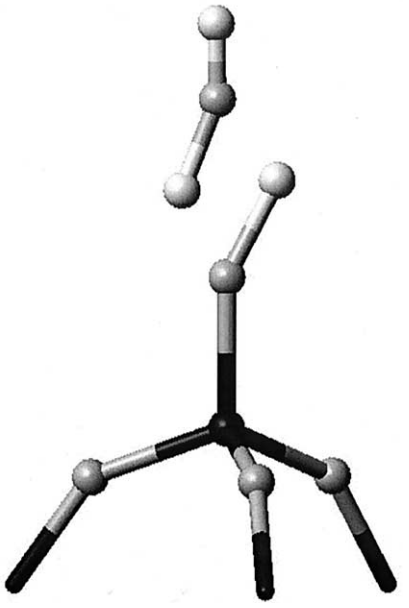

Fig. 3. Transition state configuration proposed by Kazansky et al., 1978 for hydrogen isotope exchange. Si—black, O—grey, H—white.

Figures 1c and 2b are first-order saddle points corresponding to transition states. We emphasize that these mechanisms represent those that were successfully found to have ZPECB much lower than the activation energy of silica dissolution (Rimstidt and Barnes, 1980; Dove and Crerar, 1990; Dove, 1994; Icenhower and Dove, 2000) and therefore presumably occur faster. This is under the reasonable assumption that the temperature dependent corrections to the activation energy are small. The computed ZPECB and rate constants are presented later.

The computation of specific reaction mechanisms for the n = 1 and n = 2 systems were all aborted because the reaction coordinate steps for the transition state searches were yielding relative energies exceeding the set threshold of 71 kJ/mole. Because all the possible position permutations had not been exhausted, this failure does not imply that there are absolutely no specific reaction mechanisms for the n = 1 and n = 2 systems that would have a barrier lower than the set threshold. These failed results, however, do suggest that explicit hydration is necessary to model H atom transfer reactions for aqueous solutions. The mechanism suggested by Kazansky et al. (1978) for the n = 1 system, where a transition state is formed by aligning an OH group from H_4SiO_4 and an OH group from H_2O side-by-side forming two H-bonds (Fig. 3), was among those mechanisms ruled out as being energetically unfavorable. The energy decrease due to the formation of a second H-bond is smaller than the energy increase due to the O atoms drawn into proximity of one another. Our results also suggest that water or orthosilicic acid would more readily transfer a proton to another hydroxyl group rather than share two H-bonds.

In the n = 3 and n = 7 cases, the H^+ exchange is facilitated by a Grötthus-type mechanism (Bernal and Fowler, 1933) wherein several H^+ ions concertedly transfer to neighboring molecules effecting an exchange (e.g., see Lobaugh and Voth, 1996). In both cases, this mechanism of transfer was accomplished within chains of eight alternating oxygen and hydrogen atoms forming a ring; the four oxygen and four hydrogen atoms come from three water molecules and orthosilicic acid. The exchange reaction involves one step, and the transition-state is an aquated hydronium-ion species (Figs. 1c and 2b). In the n = 3 case, the forward and reverse reaction processes are almost exact mirror images of each other, and the energies of the products and reactants are almost equal. All the transition state configurations in the study satisfy the first reaction path criterion (i.e., the transition state has one and only one imaginary frequency. See the Materials and Methods section). Checks for the second reaction path criterion (i.e., the transition state leads to both reactants and products by following the vibrational mode of the transition state that has the imaginary frequency) were performed for n = 3 at the B3LYP/6–31G(d) level and n = 7 at the B3LYP/6–31+G(d,p) level. The success in finding relatively low energy barrier paths for the n = 3 and n = 7 cases strongly suggest that surrounding water molecules are active participants in the exchange reaction and are not merely spectators to the reaction. Note that in both cases, three H_2O molecules participate in the reaction, and therefore only the n = 7 case has a true explicit hydration treatment. The transition states found have a remarkable similarity with zwitter-ions found by Smith et al. (1999) for the $(H_2O)_8$ system and suggests that a zwitter-ion may be found by changing the torsional angles of specific hydrogen atoms in our configurations. This possibility is worth looking into in the future since the existence of these may pose as alternative reaction paths.

The importance of knowing the reaction mechanism is that it allows the estimation of the isotope exchange reaction rates.

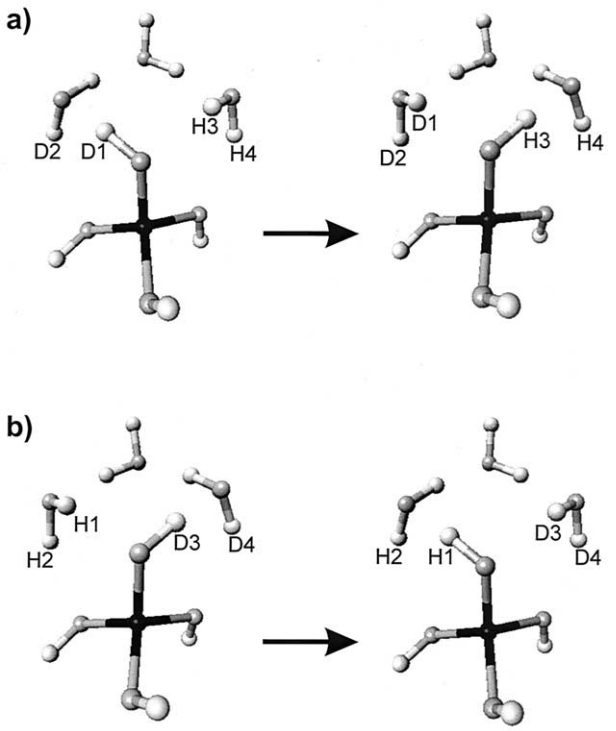

Fig. 4. Isotope exchange scheme for investigating isotope effects. Mechanisms (a) and (b) are the same reaction but in opposite directions. Odd numbered hydrogen atoms are primary H while even numbered ones are secondary H.

However, there are numerous position permutations of orthosilicic acid and multiple water molecules. Therefore, it is expected that other paths by which isotope exchange occurs possibly exist. Hence, it is not claimed that the paths described here are definitely the rate determining ones. We hypothesize, however, that any competing path should kinetically be faster than these paths to be significant contributors to the rate; the paths that we present are therefore perceived to represent lower bounds to the rate (i.e., the true k_f could only be larger or equal to what we compute).

The mechanisms depicted in Figures 1 and 2 were used to compute ZPECB and rate constants. From inspection, one can see that the reactants and products are similar but are not exactly the same. To illustrate, Figure 4 shows the exchange schemes used for the two directions in the n = 3 case. Therefore, each of the reaction mechanisms represents two isotope exchange reactions, one each for the forward and reverse directions. The slight differences in the reactant and product configurations affect ZPECB and partition functions. Thus, for calculations at the highest levels of theory used, the ZPECB were taken as the arithmetic mean

$$\Delta E_o = \tfrac{1}{2}(\Delta E_{o,f} + \Delta E_{o,r'}) \tag{14}$$

and the rate constants were taken as the geometric mean

$$k = \sqrt{k_f k_{r'}} \tag{15}$$

where the prime indicates that the appropriate isotopic substitutions have been made (see Fig. 4). Among all types of averages, the geometric mean (see e.g., Tierney, 1975) was chosen because it preserves consistency in the kinetic and

Table 1. Zero point energy corrected energies of geometry-optimized configurations and ZPECB in units of hartrees (1 hartree = 2,625 kJ/mole). Values at 6-31+G(d,p) are arithmetic means.

Reactions	B3LYP 3-21G(d)	B3LYP 6-31G(d)	B3LYP 6-31+G(d,p)	MP2 6-31+G(d,p)
$Si(OH)_4 + DOD + 2H_2O$	−807.844331	−822.150299	−822.250627	−820.393565
transition state	−817.828250	−822.129930	−822.236817	−820.370472
$Si(OH)_3OD + HOD + 2H_2O$	−817.843723	−822.150177	−822.250510	−820.393666
ΔE_o forward	0.016081	0.020369	0.013810	0.023093
ΔE_o reverse	0.015473	0.020247	0.013692	0.023194
$Si(OH)_4 + DOH + 2H_2O$	−817.840971	−822.147296	−822.247551	−820.390306
transition state	−817.824898	−822.126878	−822.233847	−820.367082
$Si(OH)_3OD + HOH + 2H_2O$	−817.840381	−822.147204	−822.247473	−820.390297
ΔE_o forward	0.016073	0.020418	0.013704	0.023224
ΔE_o reverse	0.015483	0.020326	0.013625	0.023215
$Si(OH)_4 + HOH + 2H_2O$	−817.837626	−822.129337	−822.244339	−820.386902
transition state	−817.821690	−822.110079	−822.231237	−820.362658
ΔE_o forward	0.015936	0.019258	0.013102	0.024244
$Si(OH)_4 + DOD + 6H_2O$	—	—	−1127.973522	—
transition state	—	—	−1127.95917	—
$Si(OH)_3OD + HOD + 6H_2O$	—	—	−1127.973438	—
ΔE_o forward			0.014352	
ΔE_o reverse			0.014268	
$Si(OH)_4 + DOH + 6H_2O$	—	—	−1127.970547	—
transition state	—	—	−1127.956147	—
$Si(OH)_3OD + HOH + 6H_2O$	—	—	−1127.970453	—
ΔE_o forward			0.014400	
ΔE_o reverse			0.014306	
$Si(OH)_4 + HOH + 6H_2O$	—	—	−1127.942030	—
transition state	—	—	−1127.928377	—
ΔE_o forward			0.013653	

Table 2. ZPECB in units of kJ/mole.

	B3LYP energies 3-21G(d)	6-31G(d)	6-31+G(d,p)	MP2 6-31+G(d,p)
1) $Si(OH)_4$ + DOD + $2H_2O \rightarrow Si(OH)_3OD$ + HOD + $2H_2O$				
ΔE_o forward	42.2	53.5	36.3	60.6
ΔE_o reverse	40.6	53.2	36.0	60.9
2) $Si(OH)_4$ + DOH + $2H_2O \rightarrow Si(OH)_30D$ + HOH + $2H_2O$				
ΔE_o forward	42.2	53.6	36.0	61.0
ΔE_o reverse	40.7	53.4	35.8	61.0
3) $Si(OH)_4$ + HOH + $2H_2O$ (no net change)				
ΔE_o	41.8	50.6	34.4	63.7
4) $Si(OH)_4$ + DOD + $6H_2O \rightarrow Si(OH)_3OD$ + HOD + $6H_2O$				
ΔE_o forward	—	—	37.7	—
ΔE_o reverse	—	—	37.5	—
5) $Si(OH)_4$ + DOH + $6H_2O \rightarrow Si(OH)_3OD$ + HOH + $6H_2O$				
ΔE_o forward	—	—	37.8	—
ΔE_o reverse	—	—	37.6	—
6) $Si(OH)_4$ + HOH + $6H_20 \rightarrow Si(OH)_4$ + HOH + $6H_20$ (no net change)				
ΔE_o	—	—	35.8	—

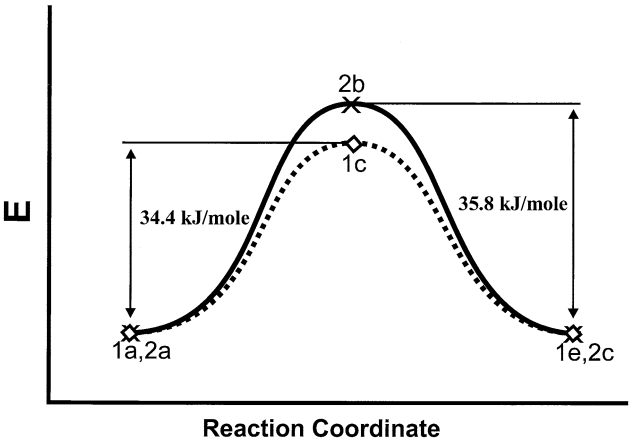

Fig. 5. Schematic diagram of the energy curves for the pure H reaction showing the location of some configurations in Figures 1 and 2 and the corresponding ZPECB for the n = 3 (hatched line, ◇) and the n = 7 (solid line, X) cases. (Note that the difference in the ZPECB is exaggerated and the energies are not drawn to scale.)

equilibrium values (e.g., the geometric mean of the equilibrium constants can be represented in terms of the geometric mean of the rate constants).

4.2. Zero-Point Energy Corrected Barriers

The ZPECB at different levels of approximation for the "simple" system, i.e., no implicit hydration, are shown in Table 1 and 2. First- and second-order kinetic isotope effects (i.e., the influence of isotopes that are participants and spectators relative to the reaction, respectively) were examined. First-order effects were evaluated by comparing two reactions such as exchanging a hydrogen atom directly involved in the reaction (i.e., the "primary" hydrogen) with deuterium (e.g., Reaction 3 vs. 2 in Tables 1 and 2),

$$Si(OH)_4 + HOH + 2H_2O \rightarrow Si(OH)_4 + HOH + 2H_2O \quad (16)$$

$$Si(OH)_4 + DOH + 2H_2O \rightarrow Si(OH)_3\,OD + HOH + 2H_2O \quad (17)$$

where Eqn. 17 shows the singly-deuterated reaction. Second-order effects were evaluated comparing two reactions such as exchanging a hydrogen atom not directly involved (i.e., the "spectator" hydrogen) with deuterium (e.g., Reaction 2 vs. 1 in Tables 1 and 2).

$$Si(OH)_4 + DOH + 2H_2O \rightarrow Si(OH)_3\,OD + HOH + 2H_2O$$
$$Si(OH)_4 + DOD + 2H_2O \rightarrow Si(OH)_3\,OD + HOD + 2H_2O \quad (18)$$

where Eqn. 18 shows the doubly-deuterated reaction. Errors in the ZPECB are introduced in the numerical cutoffs used for convergence of the solutions, and in the harmonic oscillator assumption for calculating the zero-point energies. Errors for the latter will be accounted for by scaling factors. Root mean square deviations arising from numerical errors for the energies with zero-point energy corrections are less than 10^{-8} hartrees (on the order of 10^{-2} J/mol) and are negligible compared to other corrections described later.

Computed ZPECB vary but show no apparent trend with the level of the chosen basis sets for the n = 3 system (Tables 1 and 2). Values in the B3LYP/6–31+G(d,p) level are considered the best approximations made and would be primarily used in the following discussion. (We were able to successfully compute MP2/6–31 + G(d,p) data for n = 3 but not for n = 7. However, the direction of the equilibrium for ZPECB MP2 data is opposite that of all our other calculations (Table 1) and, as we shall see later, that of experiments. Hence, we defer the discussion of the MP2 results to a latter section.)

The ZPECB at this level slightly increase from the n = 3 to the n = 7 systems (Fig. 5). This slight increase implies a slight decrease in the rate of exchange as hydration through explicit addition of water molecules is increased in the model.

In the n = 3 case, the ZPECB in both forward and reverse directions increase slightly with the exchange of a primary hydrogen with deuterium (from Eqn. 16 to Eqn. 17). This increase in ZPECB implies a decrease in reaction rate in both directions when D is involved, compared to pure H exchange. From a ZPECB of 34.4 kJ/mole, the energy is elevated to 36.0 kJ/mole for the forward reaction where deuterium is transferred from water to the orthosilicic acid and 35.8 kJ/mole for the reverse reaction.

The ZPECB in both the forward and reverse directions increase with the exchange of secondary hydrogen with deuterium (from Eqn. 17 to Eqn. 18). The reverse reaction is still slightly favored with the exchange of secondary hydrogen with deuterium.

In the n = 7 case, the replacement of primary hydrogen with deuterium (from Reaction 6 to 5 in Table 2)

$$Si(OH)_4 + HOH + 6H_2O \rightarrow Si(OH)_4 + HOH + 6H_2O \quad (19)$$

$$Si(OH)_4 + DOH + 6H_2O \rightarrow Si(OH)_3\,OD + HOH + 6H_2O \quad (20)$$

causes the ZPECB to increase in the forward and reverse directions. This implies a decrease in reaction rate in both directions when D is involved compared to pure H exchange.

Table 3. Combined ZPECB and solvation energies in units of kJ/mole and the dielectric constants used. The dielectric constants were estimated from the closest reasonable values in the CRC tables (Chemical Rubber Company, 2001).

	B3LYP/6-31+G(d,p) energies						
	298K	373K	673K	973K	1123K	1273K	1573K
1) $Si(OH)_4$ DOD + $2H_2O \rightarrow Si(OH)_3OD$ + HOD + $2H_2O$							
$\Delta E_{o,solv}$ forward	40.9	40.7	39.8	36.5	35.1	35.3	35.3
$\Delta E_{o,solv}$ reverse	40.6	40.4	39.5	36.2	34.8	35.0	35.0
2) $Si(OH)_4$ + DOH + $2H_2O \rightarrow Si(OH)_30D$ + HOH + $2H_2O$							
$\Delta E_{o,solv}$ forward	40.6	40.5	39.6	39.2	34.8	35.0	35.0
$\Delta E_{o,solv}$ reverse	40.4	40.3	39.4	36.0	34.6	34.8	34.8
4) $Si(OH)_4$ + DOD + $6H_20 \rightarrow Si(OH)_30D$ + HOD + $6H_2O$							
$\Delta E_{o,solv}$ forward	45.5	45.3	44.0	39.8	37.7	36.9	36.9
$\Delta E_{o,solv}$ reverse	45.2	45.1	43.8	39.6	37.5	36.7	36.7
5) $Si(OH)_4$ + DOH + $6H_2O \rightarrow Si(OH)_3OD$ + HOH + $6H_2O$							
$\Delta E_{o,solv}$ forward	45.6	45.4	44.1	40.0	37.8	37.0	37.0
$\Delta E_{o,solv}$ reverse	45.3	45.2	43.9	39.7	37.6	36.8	36.8
Dielectric constant	78.54	50.0	15.0	3.2	2.2	2.0	2.0
P (Mpa)	0.1	1.0	100	100	100	100	100

From a ZPECB of 35.8 kJ/mole, the forward and reverse reaction ZPECB is elevated to 37.8 kJ/mole and 37.6 kJ/mole, respectively. Hence the reverse reaction, where the orthosilicic acid produced is isotopically lighter, is more favored.

The ZPECB in both the forward and reverse reaction slightly decreases with exchange of secondary hydrogen with deuterium (from Reaction 5 to 4 in Table 2)

$$\begin{aligned} Si(OH)_4 + DOH + 6H_2O &\rightarrow Si(OH)_3\,OD + HOH + 6H_2O \\ Si(OH)_4 + DOD + 6H_2O &\rightarrow Si(OH)_3\,OD + HOD + 6H_2O \end{aligned} \tag{21}$$

Favor on the reverse reaction is maintained with the exchange of secondary hydrogen with deuterium.

In summary, the ZPECB of the isotope exchange reaction fall between 35 kJ/mole and 38 kJ/mole. The ZPECB computed indicate that the reverse reaction (H_4SiO_4 made lighter) is slightly more favored than the forward reaction. This is in agreement with experimental fractionation factors taken from water-quartz (Kuroda et al., 1982), water-rhyolitic glass systems (Dobson et al., 1989; Ihinger, 1991), and water albitic-glass systems (Dobson et al., 1989) which indicate that the silicic materials tend to be isotopically lighter than H_2O at equilibrium. This agreement will be more apparent when we present computed fractionation factors later.

The ZPECB for the n = 7 system are slightly higher than the n = 3 system by about 1 kJ/mole. We believe that orthosilicic acid in water at room temperature would resemble the n = 7 system more than the n = 3 system. However at high temperatures, it is believed to resemble the n = 3 system more, which is more gas-like in character because upon increasing the temperature, the average number of H-bonds per molecule smoothly decrease (Lokotosh et al., 2000). To our knowledge, no experimental activation energy values are known for the particular system under investigation although it is assumed that the reaction involves fast reaction kinetics (e.g., Kazansky et al., 1978).

The ZPECB found for both the n = 3 and n = 7 systems are significantly higher than the activation energy of proton transfer in water determined experimentally by Luz and Meiboom (1964), that is 10 to 12 kJ/mol, and that calculated using ab initio methods by Luth and Scheiner (1992), that is 16 kJ/mol. This can be attributed to the less acidic character of H in H_4SiO_4 compared to H in water (pK_a = 10 for H_4SiO_4 and pK_a = 7 for H_2O at 298K; see Tossell and Sahai, 2000 and references within). This result suggests that H is more mobile in water and therefore from a purely chemical standpoint (i.e., without diffusion and transport) the rate-controlling step for hydrogen isotope exchange in the H_4SiO_4-H_2O system is indeed the breaking of the H-O bond in H_4SiO_4. (While this fact may be indirectly explored by comparing bond energies, it needs to be demonstrated by comparing kinetic parameters such as energy barriers.) In other words, we can rule out proton mobility in water as a possible cause of hydrogen isotope disequilibrium if ever it occurs.

4.3. Solvation Corrections to ZPECB

ZPECB combined with solvation effects, which were evaluated using the IEFPCM model, that is $\Delta E_{o,solv}(T)$, are shown in Table 3 along with the dielectric constants used. The reactions correspond to Reactions 1, 2, 4 and 5 of Table 2. The temperatures and pressures for the dielectric constants were intended to match experimental conditions used in mineral-water exchange reaction studies (Kuroda et al., 1982; Ihinger, 1991). The results show that the effect of the solvation correction is to increase $\Delta E_{o,solv}(T)$ as T is decreased.

Similar to the simple systems, the energy barriers of reactions in the implicitly solvated systems indicate that the reverse reaction is slightly more favored for both the n = 3 and the n = 7 systems. The general trend as one decreases the dielectric constant (increase the T and pressure) is to decrease $\Delta E_{o,solv}(T)$. For the entire temperature range, $\Delta E_{o,solv}(T)$ for the n = 3 system are consistently lower than that for the n = 7 case. In the n = 3 case, $\Delta E_{o,solv}(T)$ is higher than ΔE_o below about 1000K and lower above 1000K, or $\Delta E_{o,solv}(>1000K) < \Delta E_o < \Delta E_{o,solv}(<1000K)$. In the n = 7 case, $\Delta E_{o,solv}(T)$ is higher than ΔE_o below about 1123K and lower above 1123K, or $\Delta E_{o,solv}(>1123K) < \Delta E_o < \Delta E_{o,solv}(<1123K)$. These rela-

Table 4. Temperature dependence of the TST rate constants computed using ARC and B3LYP data. Subscripts r is for the reverse reaction, f is for the forward reaction, "1" is for the singly-deuterated reaction, "2" is for the doubly-deuterated reaction, and S is for the implicitly solvated reaction. Units of k_f are in s^{-1}. Dielectric constants used for the computation of implicitly solvated reactions are in Table 3.

T(K)	k_{r1}	k_{f1}	k_{r2}	k_{f2}	k_{r1S}	k_{f1S}	k_{r2S}	k_{f2S}
n = 3								
298	8.20E+04	6.92E+04	7.10E+04	5.75E+04	1.27E+04	1.08E+04	1.10E+04	8.94E+03
373	9.89E+05	8.45E+05	8.70E+05	7.23E+05	2.33E+05	1.99E+05	2.05E+05	1.70E+05
673	5.98E+07	5.37E+07	5.49E+07	4.89E+07	3.16E+07	2.8ΔE+07	2.90E+07	2.58E+07
973	2.76E+08	2.57E+08	2.59E+08	2.40E+08	2.68E+08	2.49E+08	2.52E+08	2.33E+08
1123	4.45E+08	4.20E+08	4.22E+08	3.97E+08	5.0ΔE+08	4.76E+08	4.78E+08	4.49E+08
1273	6.51E+08	6.21E+08	6.21E+08	5.90E+08	7.15E+08	6.81E+08	6.81E+08	6.47E+08
1573	1.16E+09	1.12E+09	1.11E+09	1.07E+09	1.25E+09	1.21E+09	1.20E+09	1.16E+09
n = 7								
298	3.70E+04	3.07E+04	3.73E+04	3.06E+04	1.61E+03	1.33E+03	1.62E+03	1.33E+03
373	5.48E+05	4.60E+05	5.47E+05	4.55E+05	4.67E+04	3.92E+04	4.66E+04	3.88E+04
673	4.54E+07	4.00E+07	4.49E+07	3.94E+07	1.48E+07	1.30E+07	1.46E+07	1.28E+07
973	2.21E+08	2.02E+08	2.18E+08	2.00E+08	1.69E+08	1.55E+08	1.67E+08	1.53E+08
1123	3.56E+08	3.31E+08	3.52E+08	3.28E+08	3.55E+08	3.31E+08	3.51E+08	3.27E+08
1273	5.17E+08	4.87E+08	5.12E+08	4.82E+08	5.58E+08	5.26E+08	5.52E+08	5.20E+08
1573	9.00E+08	8.62E+08	8.90E+08	8.54E+08	9.57E+08	9.17E+08	9.47E+08	9.08E+08

tionships have significant implications on the computed rate constants as will be seen in the next section. Since $\Delta E_{o,solv}$ is closer in nature to the empirically determined activation energy, these results show how the dielectric constants influence the activation energy.

The energy barriers between the simple and implicitly solvated cases significantly differ. As observed previously, the ZPECB are also distinctly different between the n = 3 and n = 7 cases. These seem to suggest that for activation energy calculations, the treatment of solvation plays an important role.

4.4. Rates of Exchange from the Absolute Rate Constant Equation

The predicted temperature-dependent TST rate constants for the n = 3 and the n = 7 cases at the B3LYP/6 to 31 + G(d,p) level were calculated for selected temperatures from 298K to 1573K using ARC (Eqn. 3) and are shown in Table 4. Forward and reverse rate constants were considered for both the singly- and doubly-deuterated reaction mechanisms (Reactions 1, 2, 4 and 5 of Table 2) for the simple and implicitly solvated systems.

The calculations show that in the selected temperature range, the rate constants increase in magnitude from 10^4 s^{-1} to 10^9 s^{-1} for both the simple case and the solvated case and thus the reaction occurs appreciably fast in laboratory timescales. As an illustration, a rate constant of 10^4 s^{-1} implies the reaction occurs at 10000 times per second per molecular complex. To our knowledge, no experimental rate constant values are known for the particular system under investigation although it is frequently assumed that the reaction involves fast reaction kinetics. The computed rate constants imply that the rate-limiting step in real aqueous solutions is the transport and diffusion of water molecules.

The temperature dependence of the rate constants is illustrated in Figs. 6 and 7. In general, rate constants are expected to increase with temperature as observed in many experiments (Atkins, 1998). Figure 6 shows that k_f is a non-linear function of temperature. Rate constants of the singly-deuterated reaction mechanisms are consistently greater than the corresponding

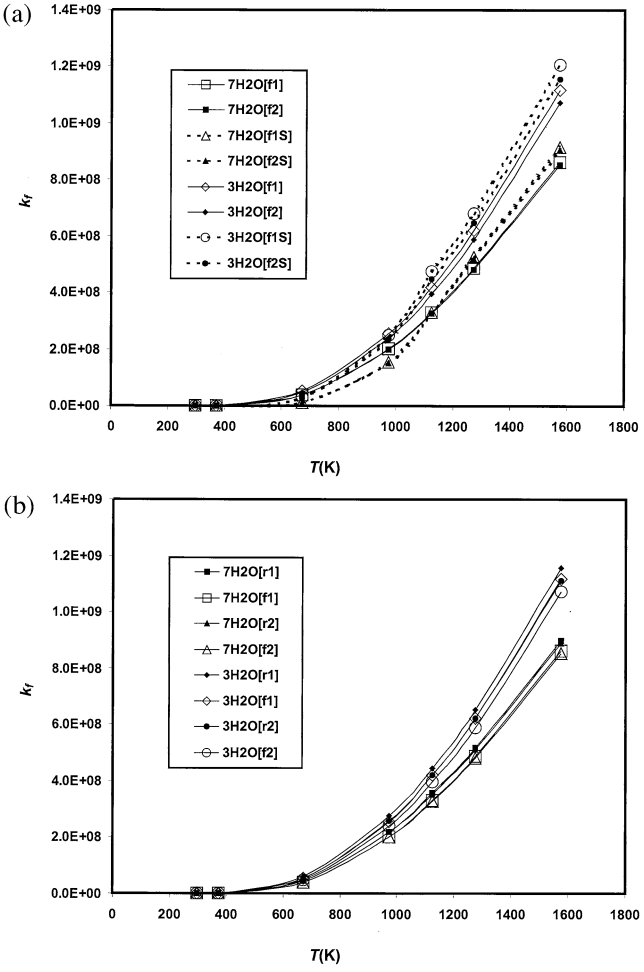

Fig. 6. Temperature dependence of MO-TST rate constants estimated using ARC with MO data at the B3LYP/6–31+G(d,p) level. Forward reaction rate constants—f, reverse reaction rate constants—b, primary isotope effect—1, secondary isotope effect—2, solvation model—s. Curves are smoothened lines to fit the points. The curves show that (a) the rate constants the singly-deuterated reactions are consistently greater than their doubly-deuterated counterpart, and (b) the rate constants for the reverse reaction are consistently lower than their corresponding forward reaction.

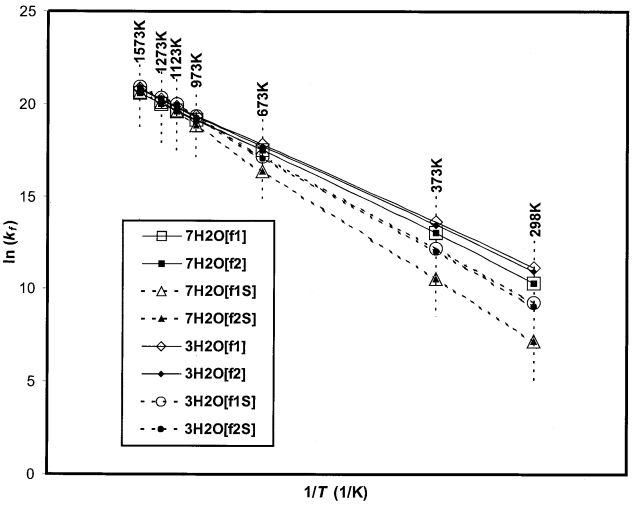

Fig. 7. $1/T$ vs. $\ln(k_f)$ diagram showing general linearity of curves. k_f are estimated using ARC with MO data at the B3LYP/6 to 31 + G(d,p) level. Forward reaction rate constants—f, reverse reaction rate constants—b, primary isotope effect—1, secondary isotope effect—2, solvation model—S. Curves are smoothened lines to fit the points.

doubly-deuterated reaction rate constants (Fig. 6a). The effect of implicit solvation is to yield rate constants lower than simple systems at low temperatures but higher at high temperatures. As discussed in the previous section, these effects are predominantly a result of the changes in the magnitude of the exponential term. Distinct groups of rate constant curves can be recognized for the n = 3 and n = 7 cases and for the simple and implicitly solvated cases. These seem to suggest that for rate constant calculations, (similar to ZPECB calculations previously discussed) the treatment of solvation is an important factor. Observe that the exponential term for the implicitly solvated system has increased by approximately 5 kJ/mol for n = 3, and 9 kJ/mol for n=7 from 298 to 1573K — this change would be imperceptible experimentally, that is in $-\ln(k_f)$ vs. 1/T plots, if the linear regression is over too wide a temperature range.

Consistent with the ZPECB of the reverse reactions (Tables 2 and 3), the calculated rate constant curves for the reverse reactions are lower than the corresponding forward reaction curves for the entire temperature range (Fig. 6b). These would have implications on the equilibrium values, which will be discussed in the next section.

In agreement with the Arrhenius relationship (see Lasaga, 1998 or Atkins, 1998 for an explanation), Figure 7 shows that the $\ln(k_f)$, vs. $1/T$ graphs are rather linear for reaction paths without the implicit solvation treatment. The $\ln(k_f)$ vs. $1/T$ graphs of the implicitly solvated reactions have slight curvature toward the high-temperature end of the plot (Fig. 7). The slopes of Arrhenius plots such as these give the negative of the activation energy. Non-Arrhenius relationships are indicative of temperature dependence in the preexponential factor and the activation energy, that is, A and E_a, respectively, in $k_f = A(T)\exp(-E_a(T)/k_BT)$. Hence, our results show that temperature dependence of the solvation, as expressed in the dielectric constant, contributes to the non-Arrhenius behavior of the rate constants.

Wigner and Eckart quantum tunneling correction coefficients are shown in Table 5. The Wigner quantum tunneling correction coefficients range from 1.91 at 298K to 1.02 at 1573K for the n = 3 case and 1.12 at 298K to 1.00 at 1573K for the n = 7 case. Hence the corrections produce a maximum of 91% change on the rate constants. It should be remarked that the correction coefficients are larger for the n = 3 case compared to the n = 7 case because of the larger imaginary vibrational mode of the former, which results in a higher frequency of conversion from reactants to products at the transition-state.

The Eckart quantum tunneling correction coefficients range from 2.56 at 298K to 1.03 at 1573K for the n = 3 case and 1.12

Table 5. Wigner and Eckart tunneling coefficients, where subscripts r is for the reverse reaction, f is for the forward reaction "1" is for the singly-deuterated reaction, "2" is for the doubly-deuterated reaction, and H is for the pure H reaction. The imaginary vibrational modes, $\nu^{\ddagger}$, for singly-deuterated, doubly-deuterated and pure H reactions are (1) For n = 3, [−941.93 cm^{-1}, −930.07 cm^{-1}], [−940.04 cm^{-1}, −927.63 cm^{-1}], and [−968.44 cm^{-1}], and (2) For n = 7, [−335.73 cm^{-1}, −353.35 cm^{-1}], [−331.32 cm^{-1}, −353.15 cm^{-1}] and [−355.75 cm^{-1}], respectively. Wigner tunneling coefficients are geometric averages and Eckart tunneling coefficients are calculated using the arithmetic mean of the frequencies.

	Wigner:			Eckart:		
T(K)	κ_1	κ_2	κ_H	κ_1	κ_2	κ_H
n = 3						
298	1.851	1.847	1.911	2.416	2.403	2.558
373	1.543	1.541	1.911	1.708	1.703	1.768
673	1.167	1.166	1.179	1.165	1.164	1.176
973	1.080	1.079	1.085	1.072	1.072	1.077
1123	1.060	1.060	1.064	1.053	1.053	1.056
1273	1.047	1.046	1.050	1.040	1.040	1.042
1573	1.016	1.016	1.017	1.025	1.025	1.026
n = 7						
298	1.115	1.085	1.122	1.119	1.118	1.127
373	1.074	1.054	1.100	1.073	1.072	1.078
673	1.023	1.016	1.024	1.021	1.021	1.022
973	1.011	1.007	1.011	1.010	1.010	1.010
1123	1.008	1.005	1.009	1.007	1.007	1.008
1273	1.006	1.004	1.007	1.005	1.005	1.006
1573	1.004	1.002	1.004	1.003	1.003	1.004

Table 6. Equilibrium constants (fractionation factors) determined computationally and experimentally. Data are from Kuroda et al. (1982), Ihinger (1991) and Dobson et al. (1989).

	n = 7				n = 3				Kuroda	Ihinger	Dobson	
T(K)	K_1	K_2	K_{1s}	K_{2s}	K_1	K_2	K_{1s}	K_{2s}	K_1	K_1	$K_{1\ rhy}$	$K_{1\ fld}$
298	0.830	0.821	0.831	0.821	0.844	0.811	0.844	0.812				
373	0.839	0.831	0.839	0.831	0.854	0.831	0.854	0.832				
673	0.881	0.879	0.881	0.879	0.899	0.891	0.899	0.892				
803											0.952	0.953
908											0.958	
973	0.917	0.916	0.917	0.916	0.932	0.928	0.932	0.928				
1023											0.962	0.966
1123	0.930	0.930	0.930	0.930	0.944	0.940	0.944	0.940		0.965	0.960	
1273	0.941	0.942	0.942	0.942	0.953	0.950	0.953	0.950				
1573	0.958	0.959	0.958	0.959	0.967	0.964	0.967	0.965	0.968			

at 298K to 1.00 at 1573K for the n = 7 case. This agrees with the findings of Truong (1997) that the Eckart coefficients are larger than the Wigner corrections particularly at low temperatures. Therefore for quantum tunneling, a reasonable upper value for the deviation is a factor of 3 for the temperature range. Note that the correction coefficients for both directions are the same and thus the direction of the equilibrium remains the same with or without the tunneling corrections.

4.5. Exchange Equilibria

The predicted temperature-dependent equilibrium constants are shown in Table 6. All values were calculated using ARC and Eqn. 11 except for those values in the last two columns, which are empirical fractionation factors for rock-mineral/water interaction obtained by Dobson et al. (1989); Ihinger (1991) and Kuroda et al. (1982). We compare our equilibrium fractionation curves with the empirical values for two main reasons. The first reason is we have not found any empirical equilibrium fractionation values for the dissolved-silica/water system. The second reason is if the computed equilibrium fractionation factors agree within a reasonable amount of error with the rock-mineral/water system, then this would suggest that the mechanisms for equilibration for the dissolved-species is similar to the rock-mineral/water system. It would also suggest that we have found a full reaction mechanism. Furthermore, if combined with the previous conclusion that rate constants are in the order of 10^4 to 10^9 s^{-1}, then it follows that there is isotopically little distinction between hydration water and bulk water (i.e., fractionation between bulk and hydration water $\alpha_{\text{bulk-hyd}} \cong 1$). Thus any large fractionations between hydration water and bulk water must be due to other factors such as transport or diffusion of water or previously trapped H isotopes in the mineral lattice.

The temperature dependence of the calculated equilibrium constants is illustrated in Figure 8, Figure 9 and Figure 10. For the entire selected temperature range, the equilibrium constants computed using rate constants indicate that the reverse reaction predominates ($K_{eq} < 1$; Table 6 and Fig. 8). The equilibrium constant increases with temperature, asymptotically approaching a value of about 1.0. The doubly-deuterated systems have consistently lower K_{eq} for the n = 3 and n = 7 cases. The n = 3 system has higher K_{eq} than the n = 7 case in general, except at lower temperatures (<400K) where the doubly-deuterated reaction n = 3 case drops lower than both the singly and doubly deuterated reactions of the n = 7 case.

For all the curves in Figure 8, the implicitly solvated and the simple systems are essentially the same, even though the rates were different as seen in Figures 6 and 7 and Table 4. Furthermore, the n = 3 and n = 7 systems yield two distinct curve trends. (Recall that the n = 7 case is our only true explicitly hydrated case.) These observations have two implications (1) the effect of implicit solvation is effectively cancelled out when equilibrium is evaluated (2) the effect of explicit hydration is significant when equilibrium is evaluated. Hence, for equilibria, explicit hydration plays a more important role than implicit hydration.

At high temperatures (Fig. 8), the calculated equilibrium constant approaches the empirically determined equilibrium constant of Kuroda et al. (1982) for quartz. However, the calculated equilibrium constants at lower temperatures are significantly lower than the experimental values for the other rock-mineral/water data. It should be pointed out though that Kuroda et al. (1982) used quartz, whereas Ihinger (1991) used

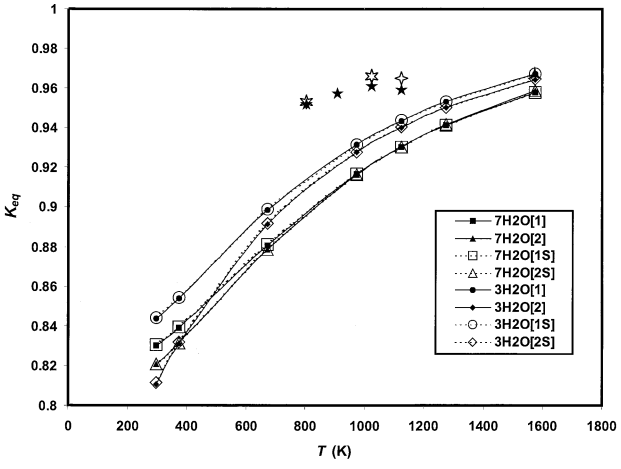

Fig. 8. Temperature dependence of MO-TST equilibrium constants. K_{eq} are calculated from k_f estimated using ARC with MO data at the B3LYP/6 to 31 + G(d,p) level. Primary isotope effect—1, secondary isotope effect—2, solvation model—S. Curves are smoothened lines to fit the points. Experimental data are from Kuroda et al. (1982) ◆, Ihinger (1991) ✧, and Dobson et al. (1989) rhyolite ★ and feldspar ☆.

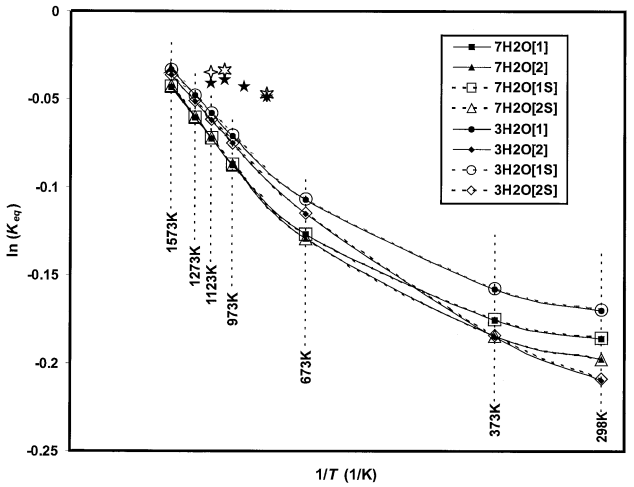

Fig. 9. $1/T$ vs. $\ln(K_{eq})$ diagram showing general non-linearity of curves. K_{eq} are calculated from k_f estimated using ARC with MO data at the B3LYP/6 to 31 + G(d,p) level. Primary isotope effect—1, secondary isotope effect—2, solvation model—S. Curves are smoothened lines to fit the points. Experimental data are from Kuroda et al. (1982) ◆, Ihinger (1991) ✧, and Dobson et al. (1989) rhyolite ★ and feldspar ☆.

rhyolitic and Dobson et al. (1989) used rhyolitic and andesitic materials. Hence, H isotope exchange is probably not occurring solely at Si-OH sites in the latter two studies. Furthermore, the pressure for the experimental results vary; the work of Kuroda et al. (1982) was at 2000 MPa, that of Ihinger (1991) at 50 MPa, and Dobson et al. (1989) at 0.14 to 0.28 MPa. The variability of the speciation, or more specifically the configuration of the water molecules in the vicinity of the exchange site appear to play a significant role in the equilibria. The equilibria is expected to ultimately result from not only the reactions depicted in Figures 1 and 2 but also the interconversion between n = 3 and n = 7 as well as other configurations not yet explored. Nevertheless, the agreement with the direction of the equilibrium is encouraging, albeit inconclusive as to the completeness of the reaction mechanism we have obtained.

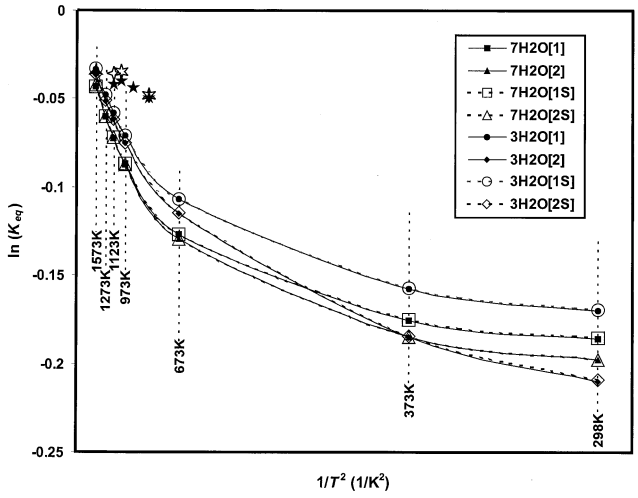

Fig. 10. $1/T^2$ vs. $\ln(K_{eq})$ diagram showing general nonlinearity of curves. K_{eq} are calculated from k_f estimated using ARC with MO data at the B3LYP/6 to 31 + G(d,p) level. Primary isotope effect—1, secondary isotope effect—2, solvation model—S. Curves are smoothened lines to fit the points. Experimental data are from Kuroda et al. (1982) ◆, Ihinger (1991) ✧, and Dobson et al. (1989) rhyolite ★ and feldspar ☆.

It is possible that the discrepancy between the fractionations may be attributed to fractionation between bulk water and hydration water. For example, if at equilibrium the fractionation between bulk water and hydration water is $\alpha_{\text{bulk-hyd}}$ and between hydration water and H_4SiO_4 is $\alpha_{\text{hyd-H4SiO4}}$, then the fractionation between bulk water and H_4SiO_4 is $\alpha_{\text{bulk-H4SiO4}} = \alpha_{\text{bulk-hyd}}\ \alpha_{\text{hyd-H4SiO4}}$. So if our computed K_1 represents $\alpha_{\text{hyd-H4SiO4}}$ (0.958 at 1573K) and if the experimental K_1 by Kuroda et al. (1982) is closer in value to $\alpha_{\text{bulk-H4SiO4}}$ (0.968 at 1573K), then this says $\alpha_{\text{bulk-hyd}} = (0.968/0.958) = 1.010$. This is worth verifying experimentally in the future, but could explain the discrepancy between our computations and experiment.

Experimental data are often extrapolated to different temperatures using the guidelines of Bigeleisen and Mayer (1947). Hence, we plotted our calculated $\ln(K_{eq})$ values versus $1/T$ and $1/T^2$ to compare with this extrapolation method. Figure 9 shows the nonlinear nature of the $\ln(K_{eq})$ vs.$1/T$ plots. The results agree with the general guidelines of Bigeleisen and Mayer (1947) (see also O'Neil, 1986) designed for diatomics

$$U = \frac{h\nu}{k_B T} \tag{22}$$

where the $\ln(K_{eq})$ vs.$1/T$ curve is predicted to be linear when $U > 20$ (low-temperature), and the $\ln(K_{eq})$ vs.$1/T^2$ curve is predicted to be linear when $U<5$ (high-temperature). The highest vibrational frequencies in our calculations is $\nu_{\max}\sim 3800\ \text{cm}^{-1}$ and thus the $\ln(K_{eq})$ vs.$1/T$ curve is predicted to be linear below 280K, and the $\ln(K_{eq})$ vs.$1/T^2$ curve is predicted to be linear above 1120K. Figure 10 shows $\ln(K_{eq})$ vs. $1/T^2$ plots; note the strongly nonlinear nature of the curves except at high temperatures (>973K). These results are generally consistent with theoretical relationship above, which has been generally verified by experimental data (O'Neil, 1986). Hence, this supports the validity of our modeling method.

4.6. Accuracy of Estimates: Scaling Factors and Anharmonicity

In this section we discuss the accuracy of the rate constants computed previously using the unimolecular harmonic oscillator approach. So far we have discussed the deviation due to Wigner and Eckart tunneling. Here we address errors arising from scaling factors (Scott and Radom, 1996) and anharmonicity.

Table 7 shows the rate constants computed using a vibrational frequency factor of 0.96 and a zero point energy correction factor of 0.98 (Foresman and Frisch, 1996). In general, the scaling factors depress the rate constants compared with the values presented in Table 4. Note that the order of the reaction is unchanged, and thus, the scaling factors do not change the previous conclusion that the isotope exchange reaction occurs at a fast rate. At lower temperatures (298K) where the effects of the scaling factors are most pronounced, the n = 3 forward

Table 7. Temperature dependence of the TST rate constants computed using a scaling factor of 0.96 for the vibrational frequency and 0.98 for the zero point energy correction and B3LYP data. Subscripts r is for the reverse reaction, f is for the forward reaction, "1" is for the singly-deuterated reaction, "2" is for the doubly-deuterated reaction. Units of k_f are in s^{-1}. Compare with Tables 4 and 6.

T(K)	k_{r1}	k_{f1}	k_{r2}	k_{f2}	K_1	K_2
n = 3						
298	6.53E+04	4.09E+04	5.6ΔE+04	3.43E+04	0.627	0.608
373	8.03E+05	5.42E+05	7.05E+05	4.66E+05	0.674	0.661
673	5.14E+07	4.06E+07	4.72E+07	3.71E+07	0.790	0.787
973	2.47E+08	2.11E+08	2.32E+08	1.98E+08	0.853	0.852
1123	4.04E+08	3.54E+08	3.83E+08	3.35E+08	0.875	0.873
1273	5.98E+08	5.33E+08	5.70E+08	5.08E+08	0.892	0.890
1573	1.08E+09	9.88E+08	1.04E+09	9.49E+08	0.916	0.915
n = 7						
298	3.11E+04	2.57E+04	3.13E+04	2.56E+04	0.826	0.818
373	4.64E+05	3.88E+05	4.63E+05	3.84E+05	0.837	0.830
673	3.97E+07	3.50E+07	3.92E+07	3.45E+07	0.882	0.881
973	1.98E+08	1.82E+08	1.96E+08	1.80E+08	0.919	0.919
1123	3.24E+08	3.02E+08	3.20E+08	2.99E+08	0.933	0.933
1273	4.75E+08	4.48E+08	4.70E+08	4.44E+08	0.944	0.944
1573	8.37E+08	8.03E+08	8.28E+08	7.96E+08	0.960	0.961

reactions with scaling factors are smaller than the calculations without scaling factors by a factor of 0.59. The n = 3 forward reaction rate constant is relatively more depressed than that of the n = 3 reverse reactions. On the other hand, the n = 7 forward and reverse reaction rate constants are approximately equally smaller by a factor of 0.84. The equilibrium constants indicate favor on the reverse reaction, similar to the calculations without scaling factors. The n = 3 equilibrium constants are depressed by a factor of 0.75 and the n = 7 equilibrium constants are roughly unchanged.

Table 8 shows the rate constants computed using the unimolecular anharmonic oscillator approach. Because anharmonicity constants for the system of interest are unavailable, we make a rough estimate of the errors in the rate constant by assuming for simplicity reasonable anharmonicity constants of $\chi_i \nu_i = 0.02 \nu_i$. (See e.g., Martin et al., 1992 for anharmonicities in water.) This assumes the anharmonicity is uniformly distributed and is proportional to the vibrational frequencies of the normal modes. While this is unrealistic and may over-account for anharmonicity, we choose this to demonstrate that the magnitude of the rate constants is not too greatly affected by large anharmonicities.

Use of the anharmonic partition function of Houston (2001) for ARC enhances the rate constants at 1573K by as much as a factor of 4.74 for the n = 3 system and by a factor of 5.39 for the n = 7 system. The equilibrium constants slightly increase at 298K by a factor of 1.02.

The largest corrections of the rate constants due to tunneling at 298K ($|2.56 - 1| = 1.56$), scaling factors at 298K ($|0.59 - 1| = 0.41$) and the use of the anharmonic oscillator model at 1573K ($|5.39 - 1| = 4.39$) taken together amount to a relative error of about (4.68 or 468%). This worst case correction is systematic, and always results in increasing the rate constants. Thus, for order-of-magnitude calculations, these corrections do not change the conclusion that the reaction occurs almost instantaneously.

Recall that the transition state partition functions are cancelled out in the evaluation of the equilibrium constants from

Table 8. Temperature dependence of the TST rate constants computed using anharmonic oscillator partition functions and B3LYP data. Subscripts r is for the reverse reaction, f is for the forward reaction, "1" is for the singly-deuterated reaction, "2" is for the doubly-deuterated reaction. Units of k_j are in s^{-1}. Compare with Tables 4 and 6.

T(K)	k_{r1}	k_{f1}	k_{r2}	k_{f2}	K_1	K_2
n = 3						
298	1.76E+05	1.51E+05	1.56E+05	1.28E+05	0.858	0.821
373	2.21E+06	1.92E+06	1.98E+06	1.66E+06	0.867	0.841
673	1.47E+08	1.34E+08	1.37E+08	1.23E+08	0.908	0.899
973	8.86E+08	8.31E+08	8.43E+08	7.87E+08	0.938	0.934
1123	1.75E+09	1.66E+09	1.68E+09	1.60E+09	0.952	0.951
1273	2.81E+09	2.70E+09	2.72E+09	2.62E+09	0.964	0.962
1573	5.47E+09	5.34E+09	5.33E+09	5.21E+09	0.977	0.978
n = 7						
298	6.95E+04	5.87E+04	7.07E+04	5.91E+04	0.844	0.837
373	1.09E+06	9.27E+05	1.09E+06	9.26E+05	0.853	0.847
673	1.03E+08	9.21E+07	1.03E+08	9.15E+07	0.892	0.890
973	7.26E+08	6.68E+08	7.20E+08	6.67E+08	0.920	0.926
1123	1.51E+09	1.42E+09	1.50E+09	1.42E+09	0.936	0.942
1273	2.45E+09	2.33E+09	2.45E+09	2.33E+09	0.950	0.954
1573	4.74E+09	4.58E+09	4.72E+09	4.60E+09	0.967	0.974

Table 9. Temperature dependence of the TST rate constants computed using ARC and MP2 data. Subscripts r is for the reverse reaction, f is for the forward reaction, "1" is for the singly-deuterated reaction, "2" is for the doubly-deuterated reaction. Units of k_f are in s^{-1}. Compare with Tables 4 and 6.

T(K)	k_{r1}	k_{f1}	k_{r2}	k_{f2}	K_1	K_2
n = 3						
298	3.64E+00	4.10E+00	3.55E+00	4.34E+00	1.127	1.222
373	3.21E+02	3.65E+02	3.13E+02	3.75E+02	1.135	1.198
673	6.41E+05	7.10E+05	6.30E+05	7.09E+05	1.108	1.125
973	1.10E+07	1.19E+07	1.09E+07	1.18E+07	1.075	1.083
1123	2.63E+07	2.80E+07	2.60E+07	2.78E+07	1.062	1.068
1273	5.19E+07	5.45E+07	5.13E+07	5.43E+07	1.052	1.057
1573	1.40E+08	1.46E+08	1.39E+08	1.45E+08	1.037	1.042

the rate constants. Therefore, the errors in the rate constants discussed above overestimate the errors in the equilibrium constants (a maximum relative error of 284%). We therefore evaluate corrections in the equilibrium constants independently from rate constant corrections. The largest corrections of the equilibrium constants (at 298K) due to scaling factors ($|0.821 - 0.608|/0.821 = 0.259$) and due to the use of the anharmonic oscillator model ($|0.830 - 0.858|/0.830 = 0.034$) taken together amount to a relative error of about (0.262 or 26.2%). If however, we take a different approach and assume that the experimental fractionations are the "true values," then the unimolecular harmonic oscillator equilibrium constant with the largest difference from the true value (i.e., at 803K) is within 7% ($|0.953 - 0.887|/0.953$) of it.

4.7. Accuracy of Estimates: MP2 Calculations

In this section we discuss implications of partial MP2 results on our B3LYP results. Although we have been successful in calculating the reaction pathway for the n = 3 system; we were unable to perform calculations on the n = 7 system due to limitations in our present computational resources. As was shown in Table 1 and 2, the ZPECB at the MP2 level are larger by almost twice as much compared to B3LYP. What is more troubling, however, is that the direction of the equilibrium is opposite to that of our B3LYP calculations and rock-mineral/water data. Table 9 shows the rate constants computed using ARC. The results show that at the selected temperature range, the rate constants increase in magnitude from 10^0 to 10^8 s^{-1}. As an illustration, a rate constant of 10^0 s^{-1} implies that the reaction occurs once per second per molecular complex. This is still relatively fast compared to the timescale of most geologic processes.

Since the equilibrium constants do not agree with experimental data, then either the model system (and hence the reaction mechanism) as shown by Fig. 1 is incorrect for the modeling the system being compared, the MP2/6–31+G(d,p) level is insufficient in accuracy, or the mechanism found is merely part of a multi-step equilibrium reaction. Because we are modeling a system in solution and comparing the results with rock-mineral/water data, the first scenario is difficult to resolve through calculations and experiments may answer this puzzle. The second and third scenario may be resolved by higher level calculations and following the reaction pathways. These issues require further investigation and are beyond the scope of the present study. It is highly possible that the successful calculation of MP2 data for the n = 7 system would resolve these issues. For example, if MP2 calculations on the n = 7 system yield rate and equilibrium constants closer to our results for B3LYP data, then we can conclude that the n = 3 data was insufficient to model the system. If however, the n = 7 rate and equilibrium constants are closer to the MP2 n = 3 system, then either the model is inappropriate for the system, the MP2/6–31+G(d,p) level is insufficient in accuracy, or the mechanism found is merely part of a multi-step equilibrium reaction. As in the B3LYP calculations, it is possible that the discrepancy between the fractionations may be attributed to fractionation between bulk water and hydration water, although $\alpha_{\text{bulk-hyd}}$ would favor the opposite direction that of B3LYP. It is very ideal therefore that the B3LYP and MP2 calculations be first reconciled.

It is commonly considered that MP2 calculations *always* give more reliable results for energies and frequency calculations than B3LYP given the same basis set. This notion however is unfounded as exemplified by the smaller scaling factors (<1) for MP2 suggested by Halls et al. (2001) and as demonstrated by the comparable calculated energies of B3LYP to MP2 (Curtiss et al., 1997). Whether MP2 or B3LYP is more reliable, both indicate that hydrogen exchange reaction can occur by the mechanism depicted in Figure 1 and that the reaction occur sufficiently fast. For most silica precipitation reactions therefore, equilibrium between orthosilicic acid and ambient water can be assumed.

5. CONCLUSION

MO-TST calculations indicate that hydrogen isotope exchange between water and H_4SiO_4 may occur through a concerted reaction within a chain of eight alternating oxygen and hydrogen atoms forming a ring. At the B3LYP/6–31+G(d,p) level, the reaction has low ZPECB consistent with a lower activation energy when compared with the dissolution of silica. The reaction furthermore describes the manner by which hydrogen ions mobilize in solution. The treatment of solvation, from the explicit addition of water molecules into the system to the application of a dielectric continuum model, yields rate constants that increasingly favor the reverse reaction. This favor on the reverse reaction is in agreement with data from rock-mineral/water system experiments.

Our B3LYP calculations yield reasonable rate constant estimates that range from 10^4 s^{-1} to 10^9 s^{-1} in the temperature range of 298K to 1573K. This suggests that diffusion and

transport of water may be the rate-limiting factor in H_4SiO_4/H_2O hydrogen isotope exchange. Tunneling corrections, scaling factors, and anharmonicity do not change the order of the rate constants. Our implicit solvation model demonstrates the contribution of the dielectric constant to non-Arrhenius behavior of the rate. The equilibrium constants computed are consistent with empirically determined equilibrium constants. Partial MP2 calculations yield significantly lower rate constants than the B3LYP results and this discrepancy requires further investigation.

Implications of fast hydrogen isotope exchange are numerous and include studies on the incorporation of hydrogen into silicate structures such as quartz or olivine. If the rates of exchange between silicic acid hydrogen and water are very fast then we need only to determine the fractionation at a given temperature to use the hydrogen isotopic composition of the incorporated hydrogen as a proxy for the hydrogen isotopic composition of the water. As we work our way through the important species in solution using the techniques developed in this paper we expect to find a whole range of exchange rates between fluids and species in solution.

Acknowledgments—The authors wish to thank the six anonymous reviewers of the manuscript for their insightful comments and suggestions, and the associate editor for his lucid synthesis of the reviews. They also thank Dr. John Tully for his very useful advice regarding the computation of reaction rates. The authors are solely responsible for any errors in the text. M. A. Felipe and D. M. Rye acknowledge the support of the National Science Foundation (NSF EAR-9628238 and EAR-9727134) and the Department of Energy (DE-FG02–01ER15216 and DE-FG02–90ER14153). J. D. Kubicki acknowledges the support of the Office of Naval Research and computational facilities provided via the DoD High Performance Computing Initiative at the Aeronautical Systems Center (Wright-Patterson AFB, Dayton OH) and at the Space and Naval Warfare Systems Center (San Diego CA).

Associate editor: J. Horita

REFERENCES

Ando K. and Hynes J. T. (1997) Molecular mechanism of HCl acid ionization in water: Ab initio potential energy surfaces and Monte Carlo simulations. *J. Phys. Chem* **101,** 10464–10478.

Atkins P. W. (1998) *Physical chemistry*, 6th ed. W.H. Freeman Co., New York.

Becke A. D. (1993) A new mixing of Hartree-Fock and local density-functional theories. *J. Chem. Phys* **92,** 1372–377.

Bernal J. D. and Fowler R. H. (1933) A theory of water and ionic solution, with particular reference to hydrogen and hydroxyl ions. *J. Chem. Phys* **1,** 515–548.

Bigeleisen J. and Mayer M. G. (1947) Calculation of equilibrium constants for isotopic exchange reactions. *J. Chem. Phys* **15,** 261–267.

Binkley J. S., Pople J. A., and Hehre W. J. (1980) Self-consistent molecular–orbital methods (21) Small split–valence basis-sets for 1st row elements. *J. Am. Chem. Soc* **102,** 939–947.

Blake R. E., ONeil J. R., and Garcia G. A. (1997) Oxygen isotope systematics of biologically mediated reactions of phosphate: I. Microbial degradation of organophosphorus compounds. *Geochim. Cosmochim. Acta* **61,** 4411–4422.

Boys S. F. and Bernardi F. (1970) Calculation of small molecular interactions by differences of separate total energies—some procedures with reduced errors. *Mol. Phys* **19,** 553–566.

Brandriss M. E., O'Neil J. R., Edlund M. B., and Stoermer E. F. (1998) Oxygen isotope fractionation between diatomaceous silica and water. *Geochim. Cosmochim. Acta* **62,** 1119–1125.

Campbell A. R., Rye D. M., and Petersen U. (1984) A hydrogen and oxygen isotope study of the San Cristobal Mine, Peru: implications of the role of water to rock ratio for the genesis of wolframite deposits. *Econ. Geol* **79,** 1387–1392.

Cancès E., Mennucci B., and Tomasi J. (1997) A new integral equation formalism for the polarizable continuum model: Theoretical background and applications to isotropic and anisotropic dielectrics. *J. Chem. Phys* **107,** 3032–3041.

Casey W. H., Lasaga A. C., and Gibbs G. V. (1990) Mechanisms of silica dissolution as inferred from the kinetic isotope effect. *Geochim. Cosmochim. Acta* **54,** 3369–3378.

Casey W. H., Phillips B. L., Karlsson M., Nordin S., Nordin J. P., Sullivan D. J., and Neugebauer-Crawford S. (2000) Rates and mechanisms of oxygen exchanges between sites in the $AlO_4Al_{12}(OH)_{24}(H_2O)_{12}{}^{7+}{}_{aq}$ complex and water: Implications for mineral surface chemistry. *Geochim. Cosmochim. Acta* **64,** 2951–2964.

Chacko T., Riciputi L. R., Cole D. R., and Horita J. (1999) A new technique for determining hydrogen isotope fractionation factors using the ion microprobe: Application to the epidote–water system. *Geochim. Cosmochim. Acta* **63,** 1–10.

Chemical Rubber Company (2001) *CRC handbook of chemistry and physics*. 82nd ed. CRC Press, Cleveland, Ohio.

Civalleri D., Garrone E., and Ugliengo P. (1998) Ab initio study of the adducts of small molecules with the isolated hydroxyl of silica and the Brønsted site in zeolites: A comparison between B3–LYP and MP2 methods. *J. Phys. Chem. B* **102,** 2373–2382.

Cole D. R. (2000) Isotopic exchange in mineral–fluid systems. IV. The crystal chemical controls on oxygen isotope exchange rates in carbonate–H_2O and layer silicate–H_2O systems. *Geochim. Cosmochim. Acta* **64,** 921–931.

Curtiss L. A., Raghavachari K., Redfern P. C., and Pople J. A. (1997) Investigation of the use of B3LYP zero–point energies and geometries in the calculation of enthalpies of formation. *Chem. Phys. Lett* **270,** 419–426.

Cygan R. T. and Kubicki J. D. (2001) Molecular modeling in mineralogy and geochemistry. Miner. Soc. Am., Washington D.C.

Dobson P. F., Epstein S., and Stolper E. M. (1989) Hydrogen isotope fractionation between coexisting vapor and silicate glasses and melts at low pressure. *Geochim. Cosmochim. Acta* **53,** 2723–2730.

Dove P. M. and Crerar D. A. (1990) Kinetics of quartz dissolution in electrolyte–solutions using a hydrotthermal mixed flow reactor. *Geochim. Cosmochim. Acta* **54,** 1267–1281.

Dove P. M. (1994) The dissolution kinetics of quartz in sodium–chloride solutions at 25°C to 300°C. *Am. J. Sci* **294,** 665–712.

Drenth W. and Kwart H. (1980) Kinetics applied to organic reactions. M. Dekker, New York.

Eckart C. (1930) The penetration of a potential barrier by electrons. *Phys. Rev* **35,** 1303–1309.

Eyring H. (1957) Statistical dynamics. Magnolia Petroleum Co., Dallas.

Faiia A. M. and Feng X. (2000) Kinetics and mechanism of oxygen isotope exchange between analcime and water vapor and assessment of isotopic preservation of analcime in geological formations. *Geochim. Cosmochim. Acta* **64,** 3181–3188.

Foresman J. B. and Frisch A. (1996) Exploring chemistry with electronic structure methods. Gaussian Inc., Pittsburgh.

Frisch M. J., Trucks G. W., Schlegel H. B., Scuseria G. E., Robb M. A., Cheeseman J. R., Zakrzewski V. G., Montgomery J. A., Stratmann R. E., Burant J. C., Dapprich S., Millam J. M., Daniels A. D., Kudin K. N., Strain M. C., Farkas O., Tomasi J., Barone V., Cossi M., Cammi R., Mennucci B., Pomelli C., Adamo C., Clifford S., Ochterski J., Petersson G. A., Ayala P. Y., Cui Q., Morokuma K., Malick D. K., Rabuck A. D., Raghavachari K., Foresman J. B., Cioslowski J., Ortiz J. V., Stefanov B. B., Liu G., Liashenko A., Piskorz P., Komaromi I., Gomperts R., Martin R. L., Fox D. J., Keith T. A., Al-Laham M. A., Peng C. Y., Nanayakkara A., Gonzalez C., Challacombe M., Gill P. M. W., Johnson B. G., Chen W., Wong M. W., Andres J. L., Head-Gordon M., Replogle E. S., and Pople J. A. (1998) Gaussian 98 (Revision A7). Gaussian, Inc., Pittsburgh.

Frisch M. J., Trucks G. W., Schlegel H. B., Gill P. M. W., Johnson B. G., Robb M. A., Cheeseman J. R., Keith T. A., Petersson G. A., Montgomery J. A., Raghavachari K., Al-Laham M. A., Zakrzewski V. G., Ortiz J. V., Foresman J. B., Cioslowski J., Stefanov B. B., Nanayakkara A., Challacombe M., Peng C.Y., Ayala P. Y., Chen W.,

Wong M. W., Andres J. L., Replogle E. S., Gomperts R., Martin R. L., Fox D. J., Binkley J. S., Defrees D. J., Baker J., Stewart J. P., Head–Gordon M., Gonzalez C., and Pople J. A. (1995) Gaussian 94 (Revision D1). Gaussian, Inc., Pittsburgh.

Geissler P. L., Dellago C., Chandler D., Hutter J., and Parrinello M. (2001) Autoionization in liquid water. *Science* **291,** 2121–2124.

Gordon M. S., Binkley J. S., Pople J. A., Pietro W. J., and Hehre W. J. (1982) Self-consistent molecular-orbital methods (22) Small split valence basis-sets for 2nd-row elements. *J. Am. Chem. Soc* **104,** 2797–2803.

Gotze J., Tichomirowa M., Fuchs H., Fuchs H., Pilot J., and Sharp Z. D. (2001) Geochemistry of agates: a trace element and stable isotope study. *Chem. Geol* **175,** 523–541.

Gregory J. K., Clary D. C., Liu K., Brown M. G., and Saykally R. J. (1997) The water dipole moment in water clusters. *Science* **275,** 814.

Gregory R. T., Criss R. E., and Taylor H. P. (1989) Oxygen isotope exchange kinetics of mineral pairs in closed and open systems—applications to problems of hydrothermal alteration of igneous rocks and precambrian iron formations. *Chem. Geol* **75,** 1–42.

Guo J. B. and Qian Y. Q. (1997) Hydrogen isotope fractionation and hydrogen diffusion in the tourmaline-water system. *Geochim. Cosmochim. Acta* **61,** 4679–4688.

Halls M. D., Velkovski J., and Schlegel H. B. (2001) Harmonic frequency scaling factors for Hartree-Fock, S-VWN, B-LYP, B3-LYP, B3-PW91 and MP2 with the Sadlej pVTZ electric property basis set. *Theor. Chem. Acc* **105,** 413–421.

Hehre W. J., Ditchfield R., and Pople J. A. (1972) Self-consistent molecular orbital methods. XII. Further extension of Gaussian-type basis sets for use in molecular orbital studies of organic molecules. *J. Chem. Phys* **56,** 2257–2261.

Hehre W. J., Radom P. R., and Pople J. A. (1986) Ab Initio Molecular Orbital Theory. Wiley, New York.

Hodges M. P. and Stone A. J. (1999) Modeling small hydronium-water clusters. *J. Chem. Phys* **110,** 6766–6772.

Hohenberg P. and Kohn W. (1964) Inhomogeneous electron gas. *Phys Rev B* **136,** B864–870.

Hoshino T. and Nishioka Y. (1999) Etching process of SiO_2 by HF molecules. *J. Chem. Phys* **111,** 2109–2114.

Houston P. L. (2001) Chemical kinetics and reaction dynamics—solutions manual. McGraw-Hill, New York.

Icenhower J. P. and Dove P. M. (2000) The dissolution kinetics of amorphous silica into sodium chloride solutions: effects of temperature and ionic effects. *Geochim Cosmochim. Acta* **64,** 4193–4203.

Ihinger P. (1991) An experimental study of the interaction of water with granitic melt. PhD dissert. 190 pp.

Janoschek R. (2001) Quantum chemical B3LYP/cc-pvqz computation of ground state structures and properties of small molecules with atoms of $Z \leq 18$ (hydrogen to argon). *Pure Appl. Chem* **73,** 1521–1553.

Jenkin G. R. T., Craw D., and Fallick A. E. (1994) Stable isotopic and fluid inclusion evidence for meteoric fluid penetration into an active mountain belt—Alpine Schist, New-Zealand. *J. Metamorph. Geol* **12,** 429–444.

Jia Y. F., Li X., and Kerrich R. (2001) Stable isotope (O, H, S, C, and N) systematics of quartz vein systems in the turbidite-hosted Central and North. Deborah gold deposits of the Bendigo cold field, Central Victoria, Australia: Constraints on the origin of ore-forming fluids. *Econ. Geol. Bull. Soc* **96,** 705–721.

Kazansky V. B., Gritscov A. M., Andreev V. M., and Zhidomirov G. M. (1978). *J. Molec. Cata.* **4,** 135–149.

Keith T. A. and Frisch, M. J. (1994) Inclusion of explicit solvent molecules in a self-consistent-reaction field model of solvation. In *Modeling the hydrogen bond* (ed. D. A. Smith) ACS Symp. Ser. **569,** 22–35.

Khan A. (1999) Theoretical studies of large $(H_2O)_{32-35}$ clusters. *J. Chem. Phys* **103,** 1260–1264.

Kohn W. and Sham L. J. (1965) Self-consistent equations including exchange and correlation effects. *Phys. Rev* **140,** 1133–1140.

Krishnamurthy R. V. and Machavaram M. (1998) Hydrogen isotope exchange in thermally stressed cellulose. *Chem. Geol.* **152,** 85–96.

Kuroda Y., Hariya Y., Suzuoki T., and Matsuo S. (1982) D/H fractionation between water and the melts of quartz, K-feldspar, albite and anorthite at high temperature and pressure. *Geochem. J* **16,** 73–78.

Lasaga A. C. (1981) Transition state theory. In *Kinetics of Geochemical Processes.* (eds. A. C. Lasaga and R. J. Kirkpatrick) *Rev. Min.* **8,** 135–170.

Lasaga A. C. (1992) Ab initio methods in mineral surface reactions. *Rev. Geophys* **30,** 269–303.

Lasaga A. C. (1998) Kinetic Theory in the Earth Sciences. Princeton University Press, Princeton.

Lasaga A. C. and Gibbs G. V. (1990) Ab initio quantum mechanical calculations of water-rock interactions: adsorption and hydrolysis reactions. *Am. J. Sci* **290,** 263–295.

Lasaga A. C. and Rye D. M. (1993) Fluid-flow and chemical-reaction kinetics in metamorphic systems. *Am. J. Sci* **293,** 361–404.

Lecluse C. and Robert F. (1994) Hydrogen isotope-exchange reaction-rates - origin of water in the inner solar-system. *Geochim. Cosmochim. Acta* **58,** 2927–2939.

Lecuyer C., Grandjean P., and Sheppard S. M. F. (1999) Oxygen isotope exchange between dissolved phosphate and water at temperatures $<=$ 135 degrees C: Inorganic versus biological fractionations. *Geochim. Cosmochim. Acta* **63,** 855–862.

Lee C. T., Yang W. T., and Parr R. G. (1988) Development of the Colle-Salvetti correlation-energy formula into a functional of the electron-density. *Phys. Rev. B* **37,** 785–789.

Lloyd R. M. (1968) Oxygen isotope behavior in sulfate-water system. *J. Geophys Res* **73,** 6099–6110.

Lobaugh J. and Voth G. A. (1996) The quantum dynamics of an excess proton in water. *J. Chem. Phys* **104,** 2056–2069.

Lokotosh T. V., Magazu S., Maisano G., and Malomuzh N. P. (2000) Nature of self-diffusion and viscosity in supercooled liquid water. *Phys. Rev. B* **62,** 3572–3580.

Longinelli A. and Nuti S. (1968) Oxygen isotopic composition of phosphorites from marine formations. *Earth Planet. Sci. Lett* **5,** 13–16.

Luth K. and Scheiner S. (1992) Calculation of barriers to proton-transfer using multiconfiguration self-consistent-field methods (1) effects of localization. *J. Chem Phys* **97,** 7507–7518.

Luz Z. and Meiboom S. (1964) Activation energies of proton transfer reactions in water. *J. Am. Chem. Soc* **86,** 4768–4769.

Martin J. M. L., François J. P., and Gijbels R. (1992) First principles computation of thermochemcial properties beyond the harmonic approximation. I. Method and application to the water molecule and its isotopomers. *J. Chem. Phys* **96,** 7633–7645.

McIver J. W. and Komornicki A. (1972) Structure of transition-states in organic reactions—general theory and an application to cyclobutene-butadiene isomerization using a semiempirical molecular-orbital method. *J. Am. Chem. Soc* **94,** 2625–2634.

McQuarrie D. A. (1973) Statistical Thermodynamics. Harper and Row, New York.

Miller W. H. (1979) Tunneling corrections to unimolecular rate constants, with application to formaldehyde. *J. Am. Chem. Soc* **101,** 6810–6814.

Mishima O. and Stanley H. E. (1998) The relationship between liquid, supercooled and glassy water. *Nature* **396,** 329–335.

Møller C. and Plesset M. S. (1934) Note on an approximation treatment for many-electron systems. *Phys. Rev* **46,** 618–622.

Odutola J. A. and Dyke T. R. P. (1980) Partially deuterated water dimmers—microwave-spectra and structure. *J. Chem. Phys* **72,** 5062–5070.

Ohmoto H. (1986) Stable isotope geochemistry of ore-deposits. In *Stable Isotopes* (eds. J. W. Valley, H. P. Taylor Jr., and J. R. O'Neil) *Rev. Min.* **16,** 491–559.

O'Neil J. R. (1986) Theoretical and experimental aspects of isotopic fractionation. In *Stable Isotopes* (eds. J. W. Valley, H. P. Taylor Jr., and J. R. O'Neil) *Rev Min.*, **16,** 1–40.

Onsager L. (1931) Reciprocal relations in irreversible processes. *I. Phys. Rev* **37,** 405–426.

Pelmenschikov A., Leszczynski J., and Pettersson L. G. M. (2001) Mechanism of dissolution of neutral silica surfaces: including effect of self-healing. *J. Chem. Phys. A* **101,** 1178–1187.

Pelmenschikov A. G., Morosi G., and Gamba A. (1997) Adsorption of water and methanol on silica hydroxylx: ab initio energy and frequency calculations. *J. Chem. Phys. A* **101,** 1178–1187.

Peng C. and Schlegel H. B. (1994) Combining synchronous transit and quasi-newton methods for finding transition states. *Israel J. Chem* **33,** 449–454.

Pople J. A., Scott A. P., Wong M. W., and Radom L. (1993) Scaling factors for obtaining fundamental vibrational frequencies and zero-point energies from HF/6-31 + G* and MP2/6-31 + G* harmonic frequencies. *Israel J. Chem* **33,** 345–350.

Rimstidt J. D. and Barnes H. L. (1980) The kinetics of silica-water reactions. *Geochim. Cosmochim. Acta* **44,** 1683–1699.

Rodriguez J., Laria D., Marceca E. J., and Estrin D. A. (1999) Isomerization, melting and polarity of model water clusters: $(H2O)_6$ and $(H2O)_8$. *J. Chem. Phys* **110,** 9039–9047.

Rybak S., Jeziorski B., and Szalewicz K. (1991) Many-body symmetry-adapted perturbation-theory of intermolecular interactions—H_2O and HF dimmers. *J. Chem. Phys* **95,** 6576–6601.

Sauer J. (1989) Molecular-models in ab initio studies of solids and surfaces—from ionic-crystals and semiconductors to catalysts. *Chem. Rev* **89,** 199–255.

Scott A. P. and Radom L. (1996) Harmonic vibrational frequencies: An evaluation of Hartree-Fock, Møller-Plesset, quadratic configuration interaction, density functional theory, and semiempirical scaling factors. *J. Phys. Chem* **100,** 16502–16513.

Sefcik J. and Goddard W. A. (2001) Thermochemistry of silicic acid deprotonation: comparison of gas-phase and solvated DFT calculations to experiment. *Geochim. Cosmochim. Acta* **65,** 4435–4443.

Shieh Y. N. and Taylor H.P. (1969) Oxygen and hydrogen isotope studies of contact metamorphism in Santa Rosa Range Nevada and other areas. *Contrib. Mineral. Petrol* **20,** 306–356.

Shmulovich K., Graham C., and Yardley B. (2001) Quartz, albite and diopside solubilities in H_2O-NaCl and H_2O-CO_2 fluids at 0.5-0.9 GPa. *Contrib. Mineral. Petrol* **141,** 95–108.

Smith A., Vincent M. A., and Hillier I. H. (1999) Mechanism of acid dissociation in water clusters: electronic structure studies of $(H_2O)_nHX$ (n = 4, 7; X=OH, F, HS, HSO_3, $OOSO_2H$, $OOHSO_2$). *J. Phys. Chem* **103,** 1132–1139.

Stanley H. E. and Teixeira J. (1980) Interpretation of the unusual behavior of H_2O and D_2O at low-temperatures-tests of a percolation model. *J. Chem. Phys* **73,** 3404–3422.

Taylor H. P. (1974) Application of oxygen and hydrogen isotope studies to problems of hydrothermal alteration and ore deposition. *Econ. Geol* **69,** 843–883.

Taylor, H. P. (1979) Oxygen and hydrogen isotope relationships in hydrothermal mineral deposits. In *Geochemistry of Hydrothermal Ore Deposits, 2nd ed* (ed. H. L. Barnes) pp. 236–277. Wiley, New York.

Taylor H. P. and Forester R. W. (1979) Oxygen and hydrogen isotope study of the Skaergaard intrusion and its country rocks—description of a 55-million-year old fossil hydrothermal system. *J. Petrol* **20,** 355–419.

Tierney J. A. (1975) Calculus and Analytic Geometry, 3rd ed. Allyn and Bacon, Boston.

Tossell J. A. and Sahai N. (2000) Calculating the acidity of silanols and related oxyacids in aqueous solutions. *Geochim. Cosmochim. Acta* **64,** 4097–4113.

Truhlar D. G., Isaacson A. D., and Garrett B. C. (1985) Generalized transition state theory. In *Theory of Chemical Reaction Dynamics*, pp. 65–137. CRC Press, Boca Raton.

Truong T. N. (1997) Thermal rates of hydrogen exchange of methane with zeolite: a direct ab initio dynamics study on the importance of quantum tunneling effects. *J. Phys. Chem. B* **101,** 2750–2752.

Valley J. W., Taylor H. P. Jr., and O'Neil J. R. (1986) *Stable isotopes*. Min. Soc. Am., Washington, D.C.

Vennemann T. W., ONeil J. R. (1996) Hydrogen isotope exchange reactions between hydrous minerals and molecular hydrogen. I. A new approach for the determination of hydrogen isotope fractionation at moderate temperature. *Geochim. Cosmochim. Acta* **60,** 2437–2451.

Walsh T. R., Wilson M., and Sutton A. P. (2000) Hydrolysis of the amorphous silica surface. II. Calculation of activationbarriers and mechanisms. *J. Chem. Phys* **113,** 9191–9201.

Wigner E. (1937) Calculation of the rate of elementary association reactions. *J. Chem. Phys* **5,** 720–725.

Xiao Y. T. and Lasaga A. C. (1994) Ab-initio quantum-mechanical studies of the kinetics and mechanisms of silicate dissolution—$H^+(H_3O^+)$ catalysis. *Geochim. Cosmochim. Acta* **58,** 5379–5400.

Xu Z. and Stebbins J. F. (1998) Oxygen site exchange kinetics observed with solid state NMR in a natural zeolite. *Geochim. Cosmochim. Acta* **62,** 1803–1809.

Xu B. L. and Zheng Y. F. (1999) Experimental studies of oxygen and hydrogen isotope fractionations between precipitated brucite and water at low temperatures. *Geochim. Cosmochim. Acta* **63,** 2009–2018.